A DOSE OPTIMIZATION STUDY IN KILOVOLTAGE CONE BEAM COMPUTED TOMOGRAPHY FOR IMAGE GUIDED RADIATION THERAPY

NUNTHAWADEE TEOCHAROEN

A THESIS SUBMITTED PARTIAL FULFILLMENT
OF THE REQUIREMENT FOR
THE DEGREE OF MASTER OF SCIENCE
(MEDICAL PHYSICS)
FACULTY OF GRADUATE STUDIES
MAHIDOL UNIVERSITY
2012

Thesis
entitled

A DOSE OPTIMIZATION STUDY IN KILOVOLTAGE CONE BEAM COMPUTED TOMOGRAPHY FOR IMAGE GUIDED RADIATION THERAPY

Nunthawadee Teocharoen
.....
Miss Nunthawadee Teocharoen
Candidate

Puangpen Tangboonduangjit
.....
Lect.Puangpen Tangboonduangjit,
Ph.D. (Medical Radiation Physics)
Major advisor

.....
Asst. Prof. Napapong Pongnapang,
Ph.D. (Medical Physics)
Co-advisor

B. Mahaisavariya
.....
Prof. Banchong Mahaisavariya,
M.D.,Dip Thai Board of Orthopedics
Dean
Faculty of Graduate Studies
Mahidol University

Puangpen Tangboonduangjit
.....
Lect.Puangpen Tangboonduangjit,
(Medical Radiation Physics)
Programme director
Master of Science Programme
in Medical Physics
Faculty of Medicine
Ramathibodi Hospital
Mahidol University

Thesis
entitled

A DOSE OPTIMIZATION STUDY IN KILOVOLTAGE CONE BEAM COMPUTED TOMOGRAPHY FOR IMAGE GUIDED RADIATION THERAPY

was submitted to the Faculty of Graduate Studies, Mahidol University
for the degree of Master of Science (Medical Physics)
on
February 13, 2012

Nunthawadee Teocharoen
Miss Nunthawadee Teocharoen
Candidate

Sivalee Suriyapee
Assoc. Prof. Sivalee Suriyapee,
M.Eng. (Nuclear Technology)
Chair

Puangpen Tangboonduangjit
Lect.Puangpen Tangboonduangjit,
Ph.D. (Medical Radiation Physics)
Member

Asst. Prof. Napapong Pongnapang,
Ph.D. (Medical Physics)
Member

B. Mahaisavariya
Prof. Banchong Mahaisavariya,
M.D.,Dip Thai Board of Orthopedics
Dean
Faculty of Graduate Studies
Mahidol University

Prof. Winit Phuapradit,
M.D., M.P.H.
Dean
Faculty of Medicine
Ramathibodi Hospital
Mahidol University

ACKNOWLEDGEMENTS

I would like to express my sincere gratitude and deeply appreciation to Lect.Puangpen Tangboonduangjit, my major advisor for her valuable advice, teaching, helpful criticisms, guidance and encouragement throughout the course of graduate program which have enabled me to carry out the study successfully. I deeply thank her for willingness in examining to improve this thesis.

I wish to deeply thank my co-advisor, Asst. Prof. Dr.Napapong Pongnapang for his comments, consultations and generous assistance.

I would like to sincere appreciation Assoc. Prof. Dr.Vipa Boonkitticharoen for her advice and comments in the research proposal.

I would like to sincere thank Assoc. Prof. Sivalee Suriyapee, Head Physicist at Division of Radiation Oncology, Department of Radiology, Faculty of Medicine, King Chulalongkorn Memorial Hospital for valuable advice in this thesis.

I am grateful for the technical help during data collection and good cooperation from all therapists, engineer and physicists in Department of Radiation Oncology, Rajavithi Hospital.

I am also thankful to all teachers, lecturers in the School of Medical Physics, Faculty of Medicine, Ramathibodi Hospital, Mahidol University, for the valuable academic knowledge on Medical Physics.

Finally, I am grateful to my family for entirely care and understanding during the entire course of study.

Nunthawadee Teocharoen

A DOSE OPTIMIZATION STUDY IN KILOVOLTAGE CONE BEAM COMPUTED TOMOGRAPHY FOR IMAGE GUIDED RADIATION THERAPY

NUNTHAWADEE TEOCHAROEN 503066 RAMP/M

M.Sc. (MEDICAL PHYSICS)

THESIS AVISORY COMMITTEE: PUANGPEN TANGBOONDUANGJIT, Ph.D. (MEDICAL RADIATION PHYSICS), NAPAPONG PONGNAPANG, Ph.D. (MEDICAL PHYSICS)

ABSTRACT

Image guided radiation therapy (IGRT) is now of interest for treatment delivery purposes. The technology provides kilovoltage cone beam computed tomography (kV-CBCT) for acquiring volumetric anatomical images to verify patient treatment positioning. Although the kV-CBCT image can improve target localization in each treatment session, this may increase the radiation absorbed dose in the patient. The aim of the present study was to evaluate the relationship between the radiation dose and various tube current-time settings by depending on the image quality for visual inspection and using a thermoluminescent dosimeter (TLD) for radiation dose measurements. The TLD-100H chips were placed on the surface and were inserted inside an anthropomorphic Rando phantom at various organs in three different sites: head and neck, chest, and pelvis. Low contrast visibility, high contrast resolution, and noise were tested using a Catphan 503 phantom. The tube current-time was based on the initial setting of the manufacturer. The relationship between the radiation doses from various tube current-time settings and the image quality were evaluated. The results indicated that the maximum organ dose was found at the rectum, at 37.1±1.4 mGy, in the pelvis protocol. The maximum skin dose was also found in the pelvis protocol at 32.0±1.7 mGy. The tube current-time was directly affected by the dose measurement with R^2 close to 1 for all cases. For image quality evaluation, the highest spatial resolution of 6 lp/cm was observed with the head and neck initial setting protocol, whereas low contrast visibility and noise increased with decreasing tube current-time setting. In clinical situations, the total tube current-time setting for image acquisition should be considered. Therefore the recommendation of the total tube current-time for optimizing the protocol of chest and pelvis scan should be 832 and 1300 mAs, respectively, while maintaining the image quality and reducing the absorbed dose by the patient.

KEY WORDS: IMAGE GUIDED RADIATION THERAPY/CONE BEAM CT/ THERMOLUMINESCENT DOSIMETER

55 pages

การศึกษาค่าปริมาณรังสีจากการถ่ายภาพด้วย KILOVOLTAGE CONE BEAM COMPUTED TOMOGRAPHY สำหรับการฉายรังสีด้วยเทคนิคภาพนำวิถี
A DOSE OPTIMIZATION STUDY IN KILOVOLTAGE CONE BEAM COMPUTED TOMOGRAPHY FOR IMAGE GUIDED RADIATION THERAPY

นันทวดี เตียวเจริญ 5036366 RAMP/M

วท.ม. (ฟิสิกส์การแพทย์)

คณะกรรมการที่ปรึกษาวิทยานิพนธ์ : พวงเพ็ญ ตั้งบุญดวงจิตร, Ph.D. (MEDICAL RADIATION PHYSICS), นภาพงษ์ พงษ์นภางค์ Ph.D. (MEDICAL PHYSICS)

บทคัดย่อ

การฉายรังสีด้วยระบบภาพนำวิถีนั้น เป็นเทคนิคที่มีการถ่ายภาพผู้ป่วยก่อนการฉายรังสีจริง โดยเครื่องเร่งอนุภาคนั้นจะมีส่วนประกอบสำคัญคือ kilovoltage cone beam computed tomography (kV-CBCT) ที่ใช้สำหรับถ่ายภาพตัดขวางผู้ป่วยแล้วเปรียบเทียบกับภาพจากเครื่องวางแผนการรักษาจึงช่วยให้กำหนดตำแหน่งการฉายรังสีได้ถูกต้องมากยิ่งขึ้น วัตถุประสงค์ของการศึกษานี้คือวัดปริมาณรังสีดูดกลืนและศึกษาความสัมพันธ์ของปริมาณรังสีดูดกลืนเมื่อปรับลดค่า mAs สำหรับภาพถ่ายลง และตรวจสอบคุณภาพของภาพจาก kV-CBCT โดยใช้ thermoluminescent dosimeter (TLD-100H) วัดปริมาณรังสีดูดกลืนในหุ่นจำลอง (anthropomorphic Rando phantom) และตรวจสอบคุณภาพของภาพด้วยหุ่นจำลอง Catphan 503 ซึ่งการวัดปริมาณรังสีนั้นแบ่งออกเป็น 3 ส่วนคือ ศีรษะและลำคอ หน้าอก และอุ้งเชิงกราน ผลการวัดปริมาณรังสีครั้งนี้พบว่า ค่าปริมาณรังสีดูดกลืนสูงสุดอยู่ที่ลำไส้ใหญ่ มีค่าเท่ากับ 3.71±0.14 cGy และปริมาณรังสีที่ผิวสูงสุด เท่ากับ 3.2±0.17 cGy การศึกษาความสัมพันธ์ระหว่างปริมาณรังสีดูดกลืนและ mAs ที่ใช้ถ่ายภาพพบว่า มีความสัมพันธ์เชิงเส้น โดย R^2 มีค่ามากกว่า 0.9 การตรวจสอบคุณภาพของภาพพบว่าการถ่ายภาพส่วนศีรษะและลำคอได้ค่า high contrast resolution และ noise มากที่สุด คือ 6 lp/cm และ 24.88 ซึ่งผลจากการลดพื้นที่การถ่ายภาพนั้นช่วยเพิ่ม high contrast resolution และลดปริมาณ noise ของภาพ จากผลการศึกษาจึงสรุปได้ว่า ค่า mAs ที่ใช้ในการถ่ายภาพนั้น มีผลต่อปริมาณรังสีดูดกลืนที่ผู้ป่วยได้รับ โดยเมื่อปรับลดค่า mAs ลงสามารถช่วยลดปริมาณรังสีดูดกลืนได้ โดยคำนึงถึงคุณภาพของภาพที่ได้

55 หน้า

CONTENTS

LIST OF TABLES

LIST OF FIGURES

LIST OF FIGURES (cont.)

LIST OF FIGURES (cont.)

LIST OF FIGURES (cont.)

LIST OF ABBREVIATIONS

Abbreviation	Term
3D-CRT	Three-dimensional conformal radiation therapy
cm	Centimeter
CT	Computed tomography
$CTDI_w$	Weighted computed tomography dose index
FOV	Field of view
HVL	Half value layer
IGRT	Image guided radiation therapy
IMRT	Intensity modulated radiation therapy
kV	Kilo voltage
kV-CBCT	Kilo voltage cone beam computed tomography
kVp	Kilo voltage peak
lp/cm	Lines pair per centimeter
mAs	Milliampere-second
MDCT	Multi-detector computed tomography
MeV	Megaelectron volt
mGy	Milli-gray
MV	Megavoltage
nC	Nanocoulomb
TLD	Thermoluminescent dosimeter

CHAPTER I
INTRODUCTION

The development of image technology strongly related to the advancement of radiation therapy. The occurrence of computed tomography (CT) in the 1970s affected to radiation therapy using image data to build a 3-dimensional (3D) patient model and design planning. Currently, three-dimensional conformal radiotherapy (3D-CRT) and intensity modulation (IMRT) techniques have been widely used for radiation therapy. 3D-CRT is a method of irradiating a tumor target volume defined in a 3D anatomical image of the patient with a set of x-ray beams individually shaped to conform to the target. The reduction in normal tissue irradiation of 3D-CRT should theoretically improve the therapeutic ratio and allow the tumor target volume to be treated to a higher dose, thereby improving the probability of tumor control. Recent technical advances in planning and delivering is intensity-modulated radiation therapy (IMRT) to provide extremely shaped radiation doses that closely conform to the tumor dimensions while sparing sensitive structures. These techniques have been shown to reduce normal tissue toxicity and to allow radiation dose to be escalated at the target (1). Therefore the development of 3DCRT and IMRT more considerable requirements of the accuracy of target treatment position as well as any variation in target position during treatment is extremely significant for the actual dose delivery. In practice, large uncertainties exist in the reproducibility of target position and the displacement of internal organs during and between fractions of radiation therapy. Consequently, the development of new technology for radiation therapy such as image-guided radiation therapy (IGRT) that used to acquire the patient's image before each treatment can be improved patient setup reproducibility.

Traditionally, the accuracy of patient setup has been verified by megavoltage (MV) radiographs. The imaging from each MV radiographs used to verify patient setup errors based on visualization and matching of bony structures, significant limitations are inherent due to the lack of soft-tissue visualization and often

poor quality. The radiographic image quality was improved by using a gantry mounted kilo-voltage (kV) X-ray source with linear accelerator to acquire the patient's image in treatment position. A new technique in IGRT is kilovoltage cone beam computed tomography (kV-CBCT) that can be used to increase the contrast for bony structure and to improve soft-tissue visualization. The combination of cone beam computed tomography and image registration software makes it possible to measure the positional error in the treatment situation directly. Although the system can provide accurate three-dimensional volumetric of the patient's anatomy for any treatment fraction, the repetition of imaging for image guidance may contribute significant dose to the patient. Moreover, the field of view (FOV) of kV-CBCT is wider than the target area of radiation treatment. Therefore, it also could increase radiation dose at the outside of the treatment field. The requirement of patient's imaging for radiation therapy should be considered with the additional dose to the patient and based on the image quality for the set up error correction. The measurement of patient dose from new modality could provide benefit data to judge using the system. The determination of patient dose from varied total tube current-time (mAs) could be contributed to the dose difference and the reduction of patient's dose should be considered while maintaining the image quality.

1.1 Imaging technique of Image Guided Radiation Therapy (IGRT)

3D-CRT and IMRT techniques are currently the standard of care in many radiotherpy clinics and are often used to further improve the therapeutic ratio through tumor dose escalation and sparing of organs at risk. This has enhanced the requirement for accurate localization of the patient, leading the way to volumetric image-guided radiotherapy IGRT, in order to assess and correct for interfractional setup error and internal organ motion (2)**.** Image-guided radiation therapy (IGRT) is the technology which uses to setup reproducibility for patients with 3D patient data. This technology is use of frequent imaging during a course of radiation therapy to improve the precision and accuracy of the delivery the treatment (3).

It is useful to review the in-room kV imaging techniques that are currently used in the community. There are three major classes:

1) Radiographic Imaging

The most basic imaging technique is the acquisition of 2D projection or planar images. Traditionally the patient's treatment position is verified by using megavoltage photon beams with film or electronic portal imaging devices such as screen, camera, ionization chambers and solid-state flat-panel detectors. The precision of MV portal imaging is limited in defining the patient's position accurately due to the inherent low contrast and two-dimensional nature of the projection images. To improve the situation, planar kV x-ray imaging has been use to provides better contrast over shorter exposure intervals than portal imaging and is rapidly being adopted as an improvement for patient setup (4).

2) Fluoroscopic Imaging

Fluoroscopic imaging is a continuous stream of planar x-ray images acquired in real time during patient setup or treatment. It allows real time monitoring and verification of treatment structures, based on visible anatomical landmarks or implanted fiducially markers. The information can be used for the management of intrafractional patient motion and organ motion and the adjustment of treatment in some cases (3).

3) Tomographic Imaging

The acquisition of many projections at different gantry angles allows the generation of volumetric CT images through various reconstruction methods. Helical CT and cone beam CT (CBCT) methods are both available with certain in-room kV imaging systems (4).

1.2 Gantry-Mounted kV Imaging Systems

Gantry-mounted kV imaging is the key feature of new medical accelerators specifically marketed for IGRT, mainly due to its in-room tomographic imaging capability at the patient treatment position. The kV imaging subsystems are mounted on the gantry orthogonal to the MV treatment and portal imaging subsystems, nominally sharing the same isocenter of the treatment radiation sources. The kV imaging system, consisting of retractable X-ray source and amorphous silicon

panel detector, is mounted orthogonally to the MV beam line of the accelerator. For CBCT image acquisition, the gantry is rotated around the patient on the treatment positioned and planar images are acquired with the kV imaging system. Volumetric image reconstruction is performed simultaneously with the acquisition to expedite the process. The reconstructed three-dimensional image from CBCT is subsequently registered with the reference image from the planning CT images.

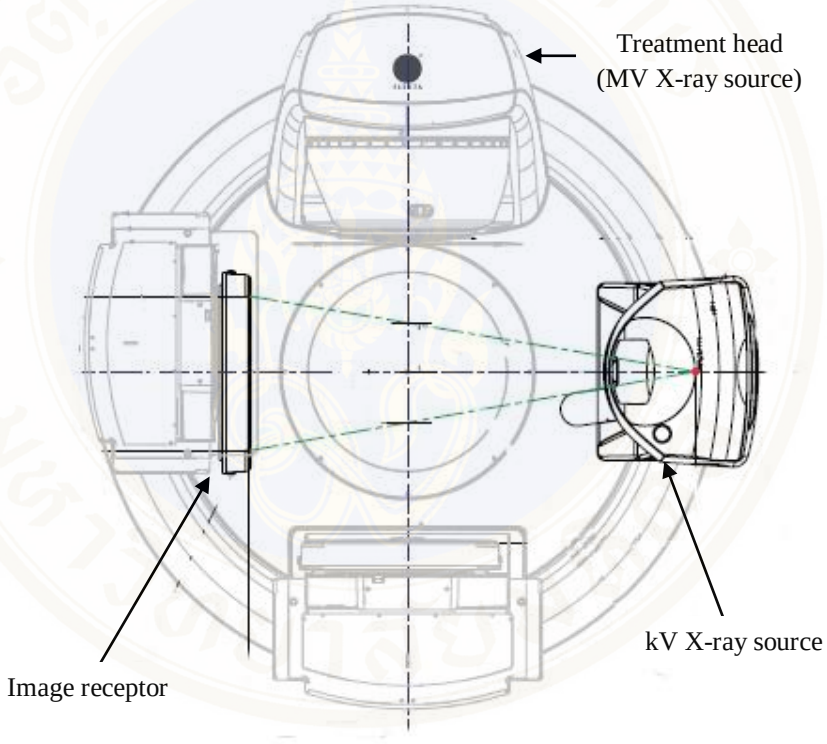

Figure 1.1 The kilovaltage cone beam computed tomography imaging system.

CHAPTER II
OBJECTIVES

The objectives of this study consist of the following.

1. To determine the organ absorbed dose from kV-CBCT in primary beam at three different sites; head and neck, chest, and pelvis by using TLD measurement in Rando phantom for initial setting protocols of the manufacturer.

2. To study the relationship between absorbed dose and total tube current-time (mAs) in kV-CBCT.

3. To study the image quality from various total tube current-time (mAs) for low contrast visibility, high contrast resolution and noise compared with the initial setting protocols from the manufacturer.

CHAPTER III
LITERATURE REVIEWS

Amer A. et al. (5) determined the organ doses in kV CBCT of the Elekta Synergy system by using TLD-100 placed on the surface and inside a Rando phantom. The organ doses were measured in three treatment sites which were the sites of head and neck, lung and pelvis. The kV CBCT scan were performed using 100 kV 38 mAs, 120 kV 152 mAs and 130 kV 456 mAs for the sites of head and neck, lung and pelvis, respectively. The maximum surface doses were 1.3, 10 and 34 mGy for head and neck, lung and pelvis, respectively and the organ dose was 1.3, 7.2 and 21 mGy for eye lens, heart and uterus, respectively. The results showed that the surface dose at pelvis was 30 mGy per scan when using in clinical situation that requires imaging on a daily basis (40 fractions), the total surface dose approaches the deterministic level of 2 Gy for transient skin erythema.

Kan M. et al. (6) studied on organ absorbed doses and effective doses from kV CBCT. All CBCT scans were performed using On-Board Imager of Varian Medical Systems. The imaging was obtained using two acquisition settings: standard mode (125 kV, 80 mA, 25 ms) and low-dose mode (125 kV, 40 mA, 10 ms). The TLD-100 chips were used for measurement by placing them on the surface and inside the female anthropomorphic phantom. Most of the organs selected were based on recommendations by the International Commission on Radiation Protection Publication 60 for effective dose determination. The maximum absorbed doses measured using the standard CBCT mode were 11.1 cGy at thyroid/thymus, 6.72 cGy at heart and 6.2 cGy at small intestine for head and neck, chest and pelvis scans, respectively. The dose data measured using low-dose mode was reduced to about one fourth and one fifth of those measured using the standard mode setting. The in-field skin doses reduced from 6.7, 6.4 and 5.4 cGy to 1.3, 1.4 and 1.2 cGy for head and neck, chest and pelvis scans, respectively.

The image quality for low-contrast resolution, spatial resolution and noise were measured by using a Catphan 600 phantom. The result for low-contrast resolution in standard mode was 4 mm in diameter at 1 % contrast. For the low-dose mode, the low contrast resolution was 5 mm in diameter at 1 % contrast which was slightly inferior to that with the standard mode. The highest spatial resolution of 9 line pairs/cm was obtained with standard mode. The CBCT image was found much noise, especially for the low-dose mode images.

Song W. et al. (7) established a comprehensive set of dose measurements data obtained from the X-ray Volumetric Imager (XVI, Elekta Oncology systems) and the On-Board Imager (OBI, Varian Medical Systems) cone beam CT systems. The weighted computed tomography dose index ($CTDI_w$) was used for reporting the radiation dose. The measured central phantom dose at different total mAs was used to verify and determine the linear relationship of dose deposited while the total mAs was increased. The relationship between the central dose and total mAs varied for the XVI protocols was a linear relationship very closely with $R^2 > 0.99$. For OBI, a linear relationship was closely with $R^2>0.99$ for all cases. The central dose was increased quite linearly while the mAs setting was increased for both units.

Kim S. et al. (8) measured the radiation dose for CBCT and multidetector computed tomography (MDCT) in terms of $CTDI_w$ and compared them with point dose measurement. The CBCT scan protocols was 125 kVp, 80 mA, 25 ms with full fan mode for head and half fan mode. The groups of TLD-100 were inserted into the cavity at center, 12, 3, 6 and 9 o'clock. It was found that $CTDI_w$ for CBCT was lower than MDCT at 35 and 49 % for head and body, respectively. The result for head scan was 89.7 ± 4 mGy. There was approximately twice that of the body scan. The radiation doses for the CBCT head scan were higher than needed for patient repositioning task in radiation treatment. The head scan protocol may need to be optimized to reduce the patient's doses.

Lehmann et al. (9) tested the image quality of Elekta Synergy with kV CBCT system. A Catphan phantom was used for image quality measurements. The phantom contains modules for resolution and low contrast measurements. For spatial resolution, three observers determined the highest resolution line-pair (lp) pattern for which the lines could be discriminated. The passing limit was set to the acceptance test

specification of 7 lp/cm. For low contrast visibility test, the image probe window was used to measure the gray values for polystyrene and the low-density polyethylene (LDPE). The measurement of low contrast visibility was adopted from the manufacturer's acceptance test. The passing limit of low contrast visibility was less than 2 %. This study, the spatial resolution was found to be able to resolve 9 lp/cm and low contrast visibility was 1.82%.

CHAPTER IV
MATERIALS AND METHODS

4.1 Materials

4.1.1 Linear accelerator machine with kV CBCT

The kV-CBCT images were acquired using X-ray Volumetric Imager (XVI) manufactured by Elekta synergy at Rajavithi Hospital as shown in Figure 4.1. The XVI system consists of a kV x-ray source and a flat-panel amorphous silicon (*a*Si cesium iodide) detector placed 90 degree to the treatment head, and shares a common axis of rotation with the MV treatment source. The detector, an active area of 41×41 cm^2 which is addressed as an array of 1024×1024 pixels was used. The images were acquired with different field of view (FOV) size. The settings of FOV use small (S) FOV for head and neck and medium (M) FOV for chest and pelvis. The geometrical FOVs are 27.68 and 42.64 cm for small and medium sizes, respectively. The cassette is inserted in front of the x-ray source to define the collimation of the beam. Each cassette has a specific length along the gantry-target axis to define the volumetric length that can be scanned. Figure 4.2 show the cassette size 10 and 20 cm were used to test image quality and the length at isocenter was 13 and 27 cm, respectively. The bowtie filter was inserted in front of the x-ray source to acquire chest and pelvis protocols (13).

Figure 4.1 Linear accelerator machine with kV-CBCT (X-ray Volumetric Imager) manufactured by Elekta synergy at Rajavithi Hospital

(a) 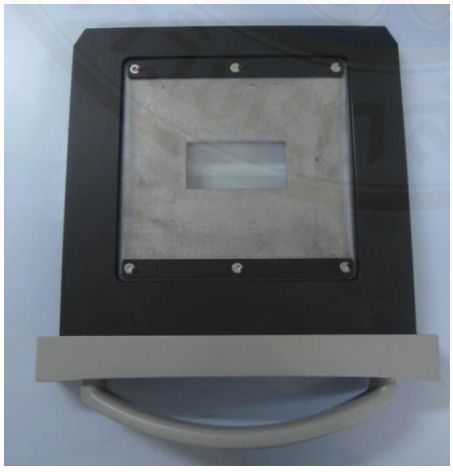 (b) 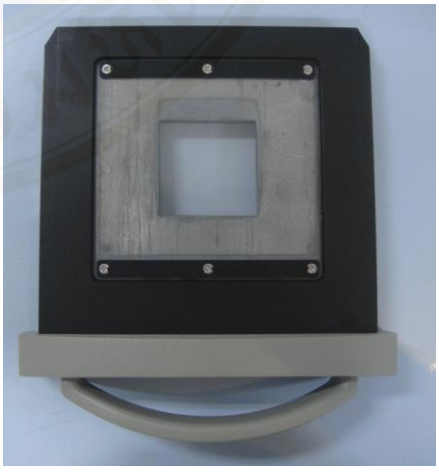

Figure 4.2 The cassette to define the length of volumetric scan for 10 (a) and 20 (b) cm.

4.1.2 Thermoluminescent dosimeters (TLDs)

Thermoluminescent dosimeters (TLDs) were used for the absorbed dose determination in Rando phantom. The TLDs used in this study was LiF:Mg,Cu,P known as TLD-100H manufactured by Bicron RMP. The TLDs are formed into chips as shown in figure 4.3 with the dimension of $3 \times 3 \times 0.8$ mm. They have a nominal density of 2.64 g/cm^3 and an effective atomic number of 8.2, closed to tissue.

Figure 4.3 The chips of thermoluminescent dosimeters (TLD-100H).

4.1.3 Thermoluminescent dosimeters system

The TLDs were read-out on a Harshaw TLD reader model 5500 (Thermo RPM, Solon, Oh) as shown in Figure 4.4. The reader is capable of reading 50 dosimeters per loading of dosimeter carrier. The Windows Radiation Evaluation and Management System (WinREM^{TM}) software was used for operating the reader. The reader uses hot nitrogen gas heating with a closed loop feedback system to produce linearly ramped temperature accurate within ± 1 ℃ to 400 ℃. The time temperature profile of the system was shown as the followings: preheat temperature 145℃ for 10 seconds, acquire temperature 260℃ for 10 seconds to acquire TL signal. The heating rate was 10 ℃/second. The TLDs were annealing to eliminate residual TL signal. The TLDs annealing oven of PTW-FREIBURG was used to anneal the TLDs. The THELDO program was used to control the annealing temperature at 260 ℃ for 10 seconds (10).

Figure 4.4 Harshaw TLD reader model 5500 (Thermo RPM, Solon, Oh)

4.1.4 Anthropomorphic Rando phantom

A female Rando phantom of The Phantom Laboratory, Salam, NY is shown in Figure 4.5 was used with TLDs to measure the absorbed doses and surface doses. The phantom is made of natural human skeletal and plastic tissue equivalent material and consists of 36 sections with the number of 0 to 35. Sections 0 to 34 are 2.5 cm thick. A section 35 is 9 cm thick. The phantom contains holes for placement of dosimeters to measure the absorbed dose inside the phantom (11).

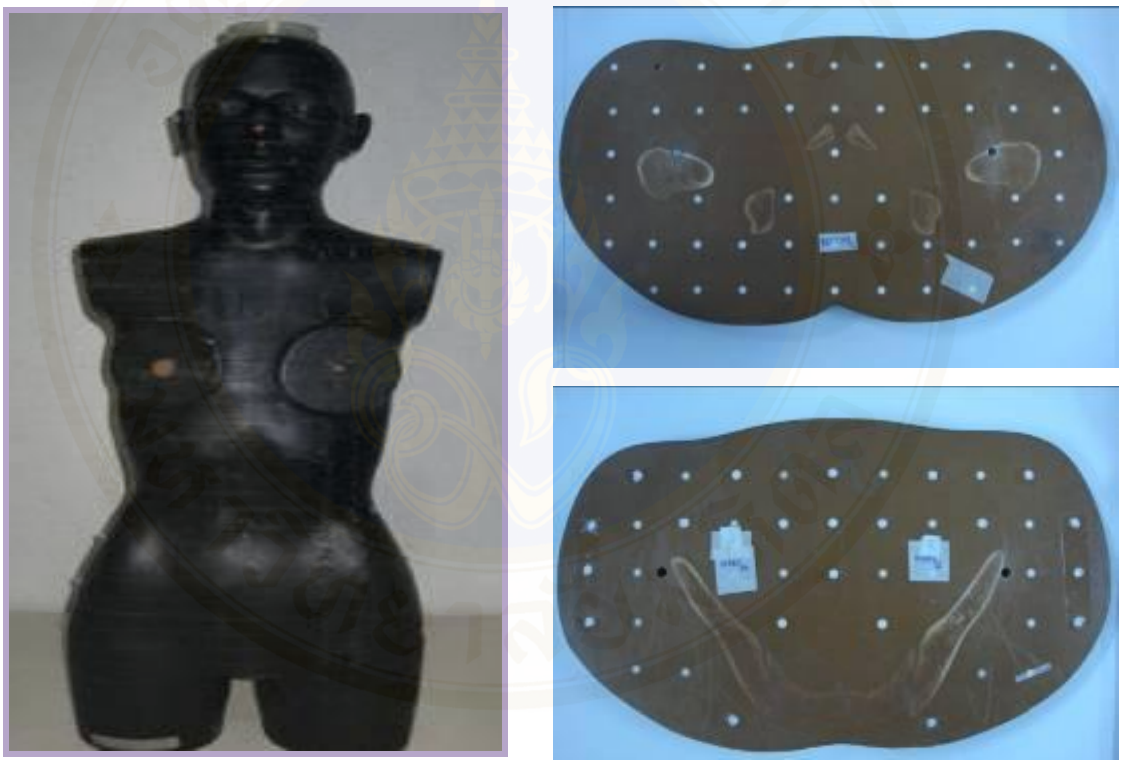

Figure 4.5 Anthropomorphic Rando phantom

4.1.5 Catphan® phantom

The Catphan® 503 phantom in Figure 4.6 manufactured by The Phantom Laboratory, Inc. was used to determine the image quality. The phantom consists of three modules namely: CTP 404, CTP 508 and CTP 486. The CTP 404 module has sensitometry target made from different materials used for low contrast visibility test. The high contrast resolution uses the CTP 508 module. This module has a 21 line pair per centimeter (line pair/cm) gauge for visual evaluation of high resolution ranging from 1 through 21 line pair/cm. The CTP 486 module is the image uniformity module made from a uniformity material. This module was used for measurement of noise value (12).

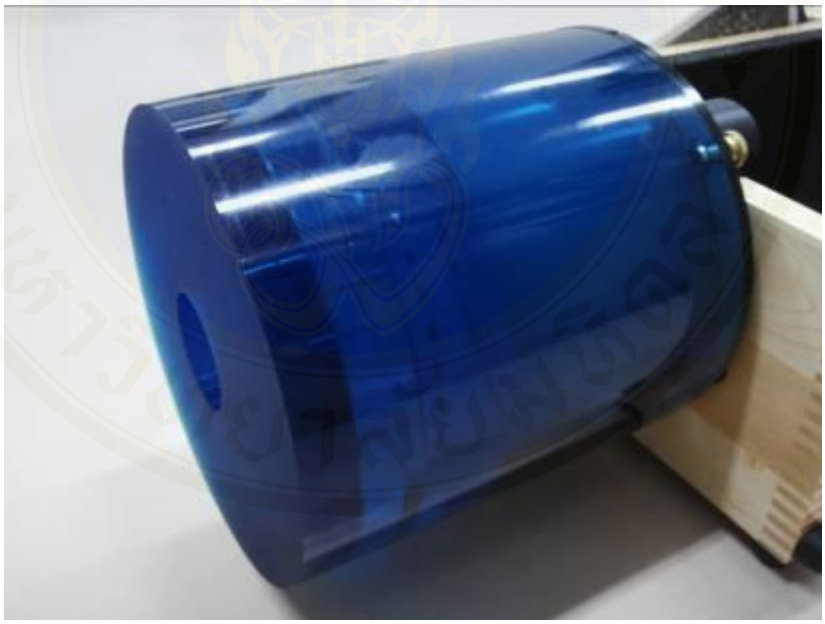

Figure 4.6 Catphan® 503 phantom for image quality test

4.1.6 Ionization chamber and electrometer

Figure 4.7 were the 6 cc ionization chamber (Radcal 9096) and radiation monitor (Accu-Pro^{TM} control unit). The ionization chamber was used to measure the absorbed dose for TLD calibration. The minimum total dose for chamber is 0.54 mR or 4.7 μGy. The ionization chamber and electrometer were calibrated by Secondary Standard Dosimetry Laboratory (SSDL) with uncertainty of calibration factor are 3.52 and 3.57 % for 100 and 120 kV, respectively.

Figure 4.7 Ionization chamber (Radcal 9096) and radiation monitor (Accu-Pro^{TM} control unit)

4.1.7 Cobalt 60 teletherapy unit machine

The source is produced by irradiating ordinary stable ^{59}Co with neutron in a reactor. The nuclear reaction can be represented by ^{59}Co (n,γ) ^{60}Co. The ^{60}Co source decay with a half-life of 5.26 years into ^{60}Ni with the emission of β particles and two photons per disintegration rays of energies 1.17 MeV and 1.33 MeV. The emitted γ rays constitute the useful treatment beam. The β particles are absorbed in the cobalt metal or the source capsule resulting in the emission of bremsstrahlung x-rays and a small amount of characteristic x-rays.

4.2 Methods

4.2.1 Absorbed dose measurement of kV-CBCT for initial setting protocols.

The kV-CBCT images were acquired using X-ray Volumetric Imager (XVI). The measurements were performed by using TLDs based on the initial setting protocols of the manufacturer; head and neck, chest and pelvis regions.

4.2.1.1 Determination of beam quality

The beam quality of kilovoltage X-ray beam requires knowledge of the photon fluence spectrum at the point of interest. The half value layer (HVL) solely or in combination with the tube potential is often used to characterize the spectrum. HVL is specified in terms of ‘‘mm Al’’ for low-energy X rays and ‘‘mm Cu’’ for medium-energy X rays. The HVL of kV-CBCT was measured for different kVp setting of 100 and 120 kVp in planar mode by using 6 cc ionization chamber (Radcal 9096) and radiation monitor (Accu-Pro^{TM} control unit). The chamber was set at the isocenter of the machine and the readings of HVL in mmAl were recorded.

4.2.1.2 TLD Preparation

TLD-100H chips were prepared for the absorbed dose measurement in anthropomorphic Rando phantom. The preparation was described as the following procedures.

a) Determination of minimum detectable dose

The minimum detectable dose of TLDs is determined by reading the residual signal of unexposed TLDs. TLDs were annealed and read for 3 times. The variation coefficient (VC) and the mean background value (BG) were used to calculate minimum detectable dose by Equation 4.1.

$$\text{Minimum detectable dose} = 3 \times VC \times BG \qquad \text{Equation 4.1}$$

b) Determination of correction factor for sensitivity

The TLDs was calculated the correction factor for sensitivity as the following procedures.

1) All TLDs were annealed at 260 ˚C for 10 second to clear the remaining exposure in TLDs.

2) The TLDs were put in acrylic plate and irradiated with known dose of 10 cGy by the cobalt-60 machine. Then they were preheat annealed with 145 ˚C for 10 second before reading

3) The time and temperature profile for acquire TL signals were setting of 260 ˚C for 23 second by the TLD reader.

4) TL signals were recorded and this process was repeated for three times.

5) The correction factor for sensitivity of each TLD was calculated by Equation 4.1.

$$\text{Correction factor for sensitivity} = \overline{Q}/Q_i \qquad \text{Equation 4.1}$$

where $\overline{Q}$ is average reading of all TLDs

Q_i is reading of each TLD

c) Linearity test of TLDs

The linearity of all TLDs was checked by exposing known dose with X-ray from kV-CBCT in planar mode. TLDs were exposed with the known dose of 0.5, 2, 4 and 5 cGy for both 100 and 120 kVp. The process was repeated three times and the readings were averaged. The relationship between known dose and TL signal were determined.

d) TLD calibration

TLDs were calibrated with 6 cc ionization chamber and used kV-CBCT in planar mode for 100 and 120 kVp. The TLD calibration was described as the following procedures.

1) Ionization chamber was used to measure the exposure in air at the isocenter of machine. The exposure was measured for 100 and 120 kVp and with various mAs values to calculate different absorbed dose.

2) The absorbed dose in water was calculated according to Equation 4.2.

$$\text{Absorbed dose in free space} = \text{Reading} \times N_K F \left[\left(\frac{\mu_{en}}{\rho} \right)^{w}_{air} \right]_{air} \qquad \text{Equation 4.2}$$

where Reading is the electrometer reading in Roentegen (R)

N_k is the air kerma calibration factor for the ion chamber in Roentgen (R)

F is the conversion factor to convert exposure to absorbed dose (0.00876 mGy/mR)

$\left[\left(\frac{\mu_{en}}{\rho}\right)^{w}_{air}\right]_{air}$ is the ratio of mass energy absorption according to TG61 protocol

3) The TLDs were exposed with the same setting as the ionization chamber by put them on the Styrofoam at the isocenter of the machine and were calibrated with the same condition as the measurement of absorbed dose by using ionization chamber. The readings of TLDs were average and multiplied with the correction factor of sensitivity for each TLD.

4) The readings of TLDs (nC) were plotted against the absorbed dose (cGy).

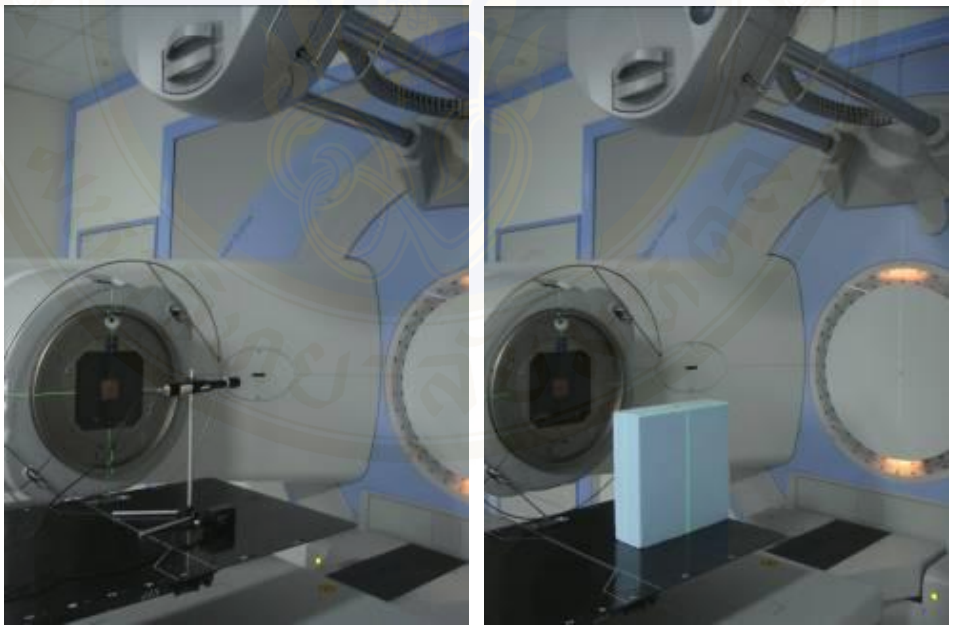

Figure 4.8 The setting of ionization chamber and TLDs on the Styrofoam for the TLDs calibration.

4.2.1.3 Absorbed dose measurement in anthropomorphic Rando phantom

The absorbed dose in organs was measured in anthropomorphic Rando phantom by using TLDs. The TLDs were placed on surface and in organs of interest for three different sites; head and neck, chest and pelvis as described in the following processes.

a) TLDs were encapsulated in plastic tube by using two TLDs per one plastic tube and used to insert in Rando phantom. The surface dose was measured by using plastic sac filled of two TLDs which taped on surface of Rando phantom. For head and neck, the dose was measured at eye lens, thyroids and skin. For chest, the dose was measured at heart, breasts and skin. And pelvis, the dose was measured at ovaries, rectum and skin. For skin dose, TLDs were placed in primary beam at anterior, posterior, right lateral and left lateral.

b) The Rando phantom was scanned according to initial protocol for the machine for three parts of phantom as the following Table 4.1. The measurement was repeated three times for each treatment site.

c) TLDs signal were read and averaged for each organ. The TLD readings were multiplied by the correction factor for sensitivity of each TLD and use the calibration factor converted these TL signal to absorbed dose.

Table 4.1. The acquisition setting for initial protocols of head and neck, chest and pelvis

Parameters	**Protocols**		
	Head and neck	**Chest**	**Pelvis**
kVp	100	120	120
Total mAs	36.1	1040	1664
No. of frames	360	650	650
Collimator size	S20	M20	M20
FOV	27.68 (S)	42.64(M)	42.64(M)
Acquisition angle	350-170	180-180	180-180

S = small size and M = medium size

4.2.2 Determination of the relationship between absorbed dose and total tube current-time (mAs)

The total tube current-time (mAs) setting in initial protocol for chest and pelvis were reduced to three steps as shown in Table 4.2. For head and neck, the mAs of 36.1 for initial setting was the lowest value of the machine so the absorbed dose was measured only this mAs value. The absorbed dose was measured by using thermoluminescent dosimeter (TLD) in the anthropomorphic Rando phantom on surface and in organs of interest the same as the absorbed dose measurement for initial protocols. The dose was measured for various mAs setting to determine the relationship between total tube current-time (mAs) setting and absorbed dose. The averaged dose for each organ was plotted as the function of mAs setting value for chest and pelvis sites.

Table 4.2 The total mAs setting of the various mAs protocol for determination of the relationship between total mAs and absorbed dose.

Site of scan	**Total mAs**			
	1 (100%)	**2 (≈75%)**	**3 (≈50%)**	**4 (≈25%)**
Head and neck	36.1	-	-	-
Chest	1040	832	520	260
Pelvis	1664	1300	832	416

4.2.3 Image quality test

Image quality test was performed by using Catphan® 503 phantom to determine the low contrast visibility, high contrast resolution and noise of kV-CBCT image. The phantom was placed on the gantry end of the table and using room lasers to align the markers dot of phantom as shown in Figure 4.7. The image quality test was performed by using all mAs settings that used for the dose measurement in Rando phantom and using two collimator sizes; 10 and 20 cm in length. The image quality was evaluated and compared in kV-CBCT images from initial setting protocols and various tube current–time (mAs) protocols as shown in Table 4.3. The image was analyzed as the following processes.

Table 4.3 The mAs setting for image quality test of three different site protocol.

Site of scan	mAs setting	Collimator size (cm)	
Head and neck	36.1	10	20
Chest	1040	10	20
	832	10	20
	520	10	20
	260	10	20
Pelvis	1660	10	20
	1300	10	20
	832	10	20
	416	10	10

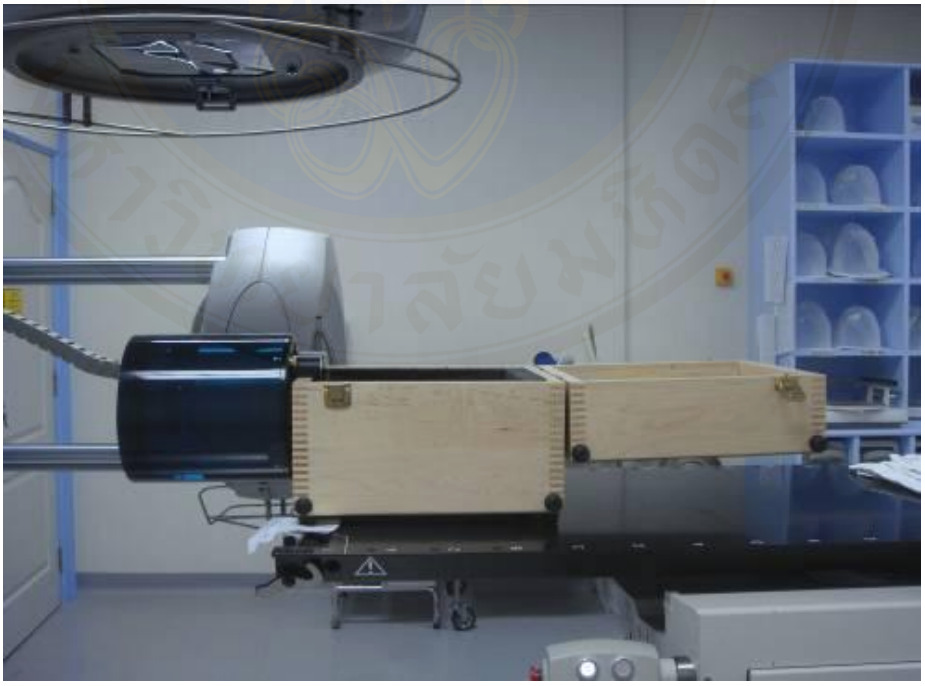

Figure 4.9 The alignment of Catphan®503 phantom in kV-CBCT system.

4.2.3.1 Low contrast visibility

Low contrast visibility was analyzed as the procedure of customer acceptance test for X-ray volume imager.

a) Select the slice of CTP 404 module until the orientation markers shown in Figure 4.8 are aligned vertically and horizontally.

b) The mean and standard deviation of pixel value was measured at polystyrene and low density polyethylene by using region of interest size of 0.35 cm.

c) Calculate the low contrast visibility by Equation 4.3.

$$\text{Low contrast visibility } \% = \frac{(CT_{polystyrene} - CT_{LDPE})/10}{\left\{\frac{Mean_{polystyrene} - Mean_{LDPE})}{(SD_{polystyrene} + SD_{LDPE})/2}\right\}} \quad \text{Equation 4.3}$$

where $CT_{polystyrene}$ is the estimation value of CT number at polystyrene

CT_{LDPE} is the estimation value of CT number at low density polyethylene (LDPE)

$Mean_{polystyrene}$ is the averaged value of CT number from measurement at polystyrene

$Mean_{LPDE}$ is the averaged value of CT number from measurement at LPDE

$SD_{polystyrene}$ is the standard deviation of CT number from measurement at polystyrene

SD_{LPDE} is the standard deviation of CT number from measurement at LPDE

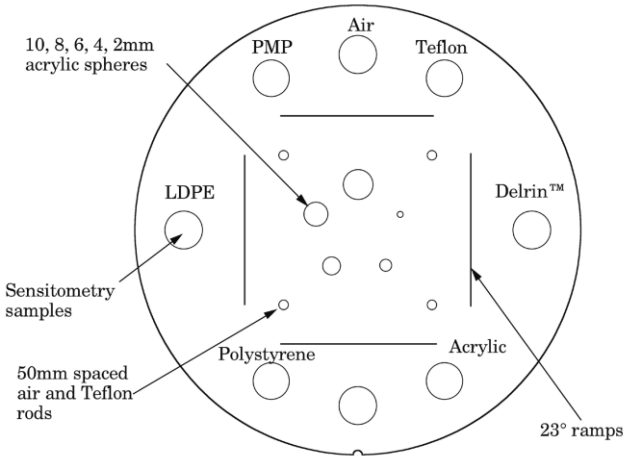

Figure 4.10 Transverse image of CTP 404 Module of Catphan® 503 phantom.

4.2.5.2 High contrast resolution

The image of bar pattern was analyzed for high contrast resolution as the following procedures.

a) The middle slice for spatial resolution in CTP528 module as shown in Figure 4.9 was selected.

b) Establish the highest number of line pair that is visible and record the value.

c) Determine the high contrast resolution for image from initial setting protocols and various mAs settings.

Figure 4.11 Transverse image of CTP 528 Module of Catphan® 503 phantom.

4.2.3.3 Noise

Noise was measured with the uniformity module of the Catphan® phantom in order to express the standard deviation of the pixel value taken from the image of the uniform inserts. Region of interest was set of 2.5 cm and the measurement was repeated three times. The value was averaged and recorded.

CHAPTER V
RESULTS AND DISCUSSION

5.1 Absorbed dose measurement of kV-CBCT for initial setting protocols.

5.1.1 Determination of beam quality

The kVp setting for TLDs calibration and dose measurement used 100 kVp for head and neck and 120 kVp for chest and pelvis. The HVL value was used to determine the ratio of mass energy absorption according to TG61 protocol for calculating the absorbed dose in water. The half value layer in terms of millimeter of aluminum of X-ray volume imager in planar mode for 100 and 120 kVp was 6.3 and 7.3 mmAl, respectively.

5.1.2 TLDs preparation

TLDs were prepared for the absorbed dose measurement of the detectable minimum dose, the correction factor for sensitivity, linearity and the absorbed dose calibration.

5.1.2.1 Determination of minimum detectable dose

The averaged background of all TLDs is 0.2 nC (0.75 mGy) and the variation coefficient is 0.11 nC. Therefore, the minimum detectable dose is 0.13 nC, according to equation 4.1. Then the absorbed dose was calculated by using equation from calibration curve. The minimum detectable dose for the absorbed dose measured by TLDs is 0.15 mGy.

The minimum value for this study was 0.9 mGy so the measured dose was higher than the detectable minimum dose of 0.15 mGy.

5.1.2.2 Determination of the correction factor for sensitivity

The correction factor for sensitivity of each TLD was shown in Table A1 in the Appendix. The TLDs that used for the absorbed dose measurement have correction factor for sensitivity values varied from 0.9206 - 1.0996 and the coefficient of variation was 4.9%.

5.1.2.3 Linearity test of TLDs

The relationship between known dose and TL signal was shown in Figure 5.1 and 5.2 for 100 and 120 kVp, respectively. The known doses of 5, 20, 40 and 50 mGy were plotted with the TL signal. The relationship was a linear relation with excellent R^2 which were 0.99 and 0.99 for 100 and 120 kVp, respectively.

5.1.2.4 TLD calibration

The calibration curves as shown in Figure 5.1 and 5.2 were determined for 100 and 120 kVp. The corrected charge of TLD (nC) were plotted against the irradiated dose (cGy) of 0.5, 2.1, 3.2, 4.2 and 5.3 cGy for 100 kVp and 0.5, 2.2, 3.2, 4.2 and 5.2 cGy for 120 kVp. The linear relationship can be found as the linear equations with excellent R^2.

The linear equations in Figure 5.1 and 5.2 used to calculate absorbed dose from corrected charged of TLDs are $Y=0.017X + 0.013$ for 100 kVp and $Y=0.017X + 0.075$ for 120 kVp where Y is absorbed dose in cGy and X is the corrected charge (nC) by the correction factor of sensitivity.

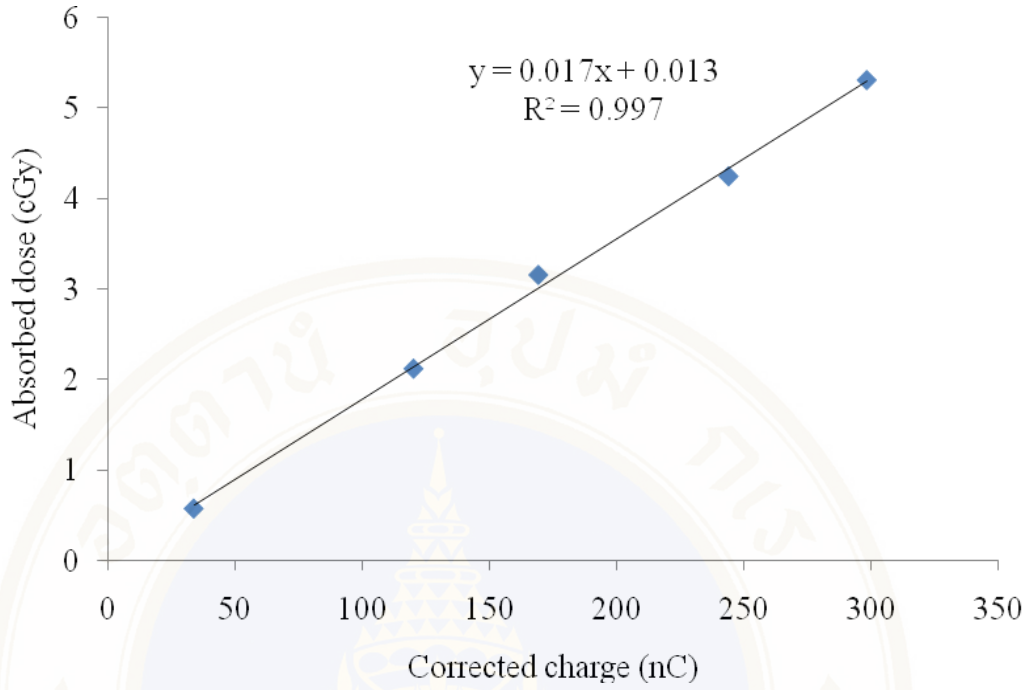

Figure 5.1 The calibration curve of corrected charge (nC) for absorbed dose (cGy) of 100 kVp.

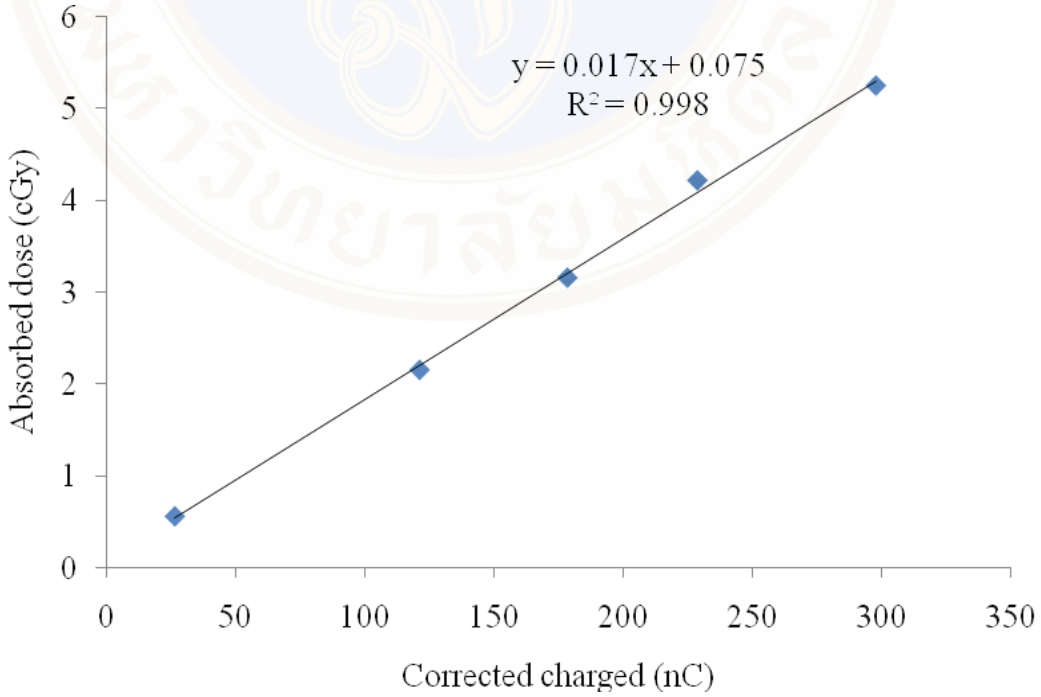

Figure 5.2 The calibration curve of corrected charge (nC) for absorbed dose (cGy) of 120 kVp.

5.1.3 Absorbed dose measurement in anthropomorphic Rando phantom

The kV-CBCT images for the position of absorbed dose measurement were shown in Figure 5.3 and 5.4. Table 5.1-5.3 represent the organ dose and skin dose from the initial setting protocols of the machine for head and neck, chest and pelvis scan. The dose was measured for the organ and skin in primary beam. For head and neck, the maximum dose was found at thyroids of 1.3 mGy and the averaged skin dose was 1.3 mGy. Chest scan showed the maximum dose of 32.2 mGy at heart and 25 mGy of the averaged skin dose. For pelvis scan, the maximum dose was 38 mGy at rectum and the averaged skin dose was 33.8 mGy

The measured organ and skin dose for head and neck at the right site was lower than those at the left site. The reason is that the acquisition setting of head and neck protocol using 180º and angle for image acquisition was 350º to 170º thus right eye len and right lateral skin is less X-ray exposure.

For clinical respect, a large volume of the normal tissue is involved in the cone beam CT imaging and the repeated use in treatment course with 35 fractions for dose delivery on a daily basis may contribute significant dose to normal tissue. Therefore the study of dose from imaging for setup error correction is important. The maximum averaged skin dose for initial protocol was 33 mGy at pelvis. So the total additional dose in 35 fractions from imaging at skin could be 1.2 Gy. However the total surface dose does not approach the deterministic level of 2 Gy/fraction for transient skin erythema (14).

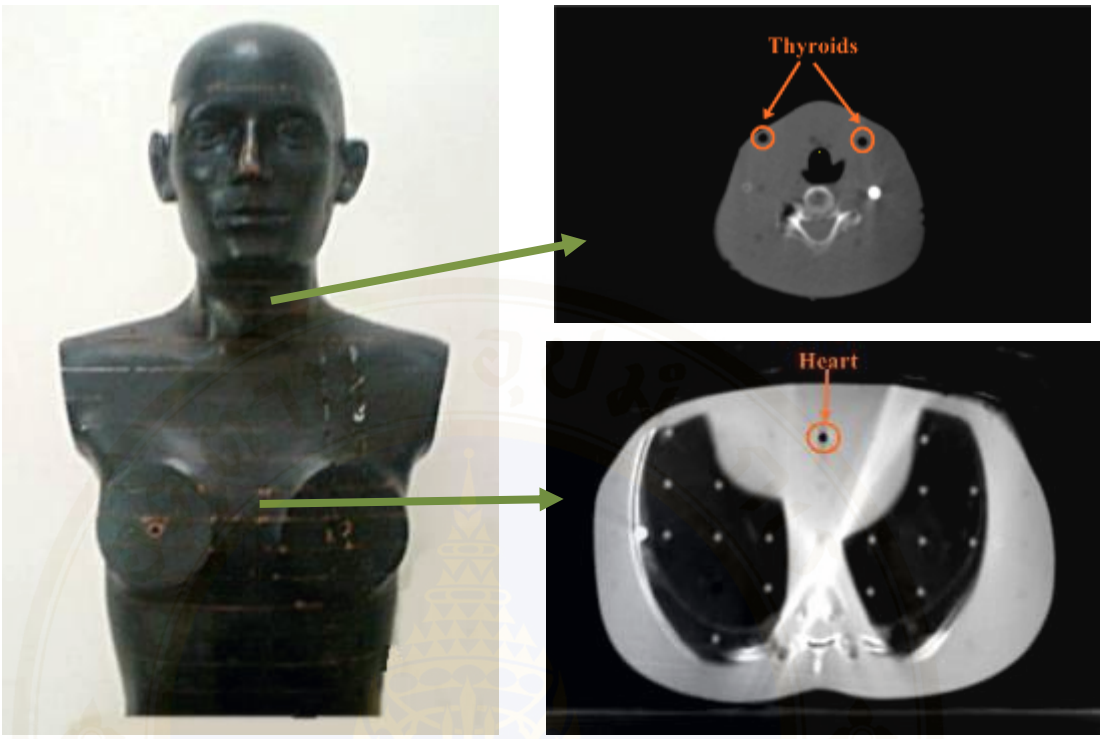

Figure 5.3 The kV-CBCT images for positions of measured dose at thyroids and heart in Rando phantom.

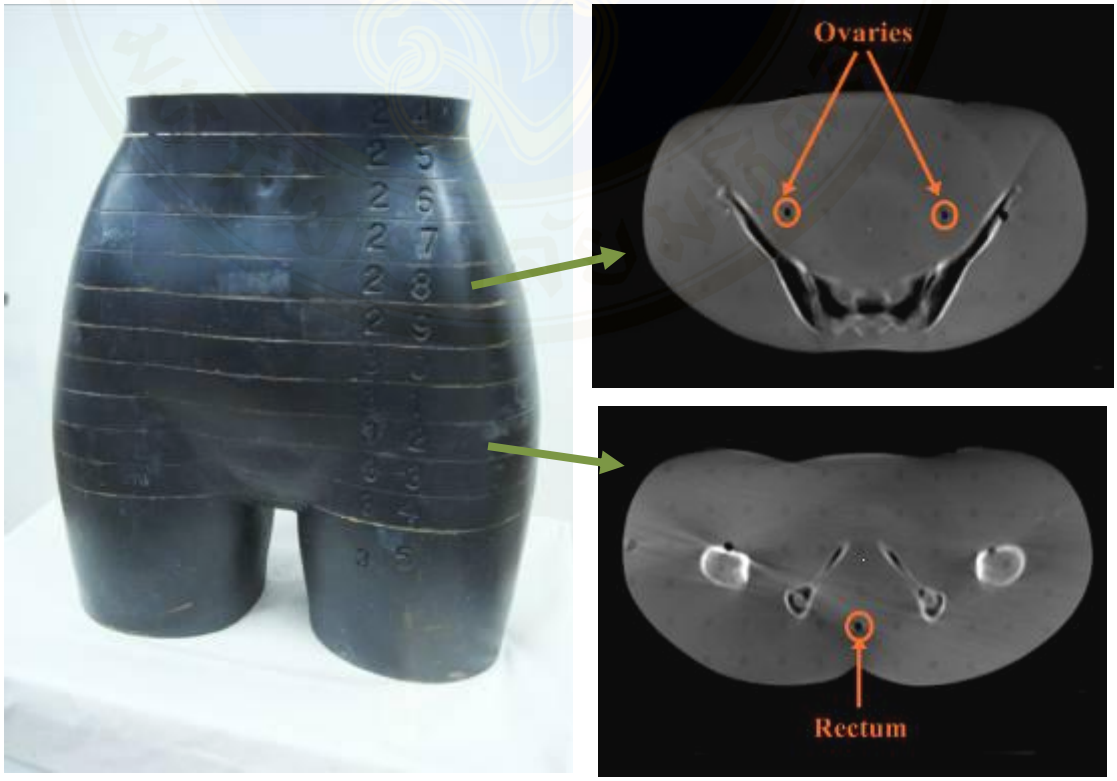

Figure 5.4 The kV-CBCT images for positions of measured dose at ovaries and rectum in Rando phantom.

Table 5.1 The measured absorbed dose of head and neck for initial setting protocol (36.1 mAs).

Position	**Mean absorbed dose (mGy ± SD)**
Thyroid	1.25 ± 0.02
Right eye len	0.88 ± 0.01
Left eye len	1.36 ± 0.04
Anterior skin	1.24 ± 0.07
Right lateral skin	0.72 ± 0.07
Left lateral skin	1.82 ± 0.07
Posterior skin	1.25 ± 0.05
Average Skin	1.26 ± 0.01

Table 5.2 The measured absorbed dose of chest scan for initial setting protocol (1040 mAs).

Position	**Mean absorbed dose (mGy ± SD)**
Heart	32.2 ± 1.0
Right breast	27.0 ± 0.4
Left breast	22.2 ± 0.4
Anterior skin	27.6 ± 1.1
Right lateral skin	24.6 ± 1.2
Left lateral skin	21.1 ± 1.0
Posterior skin	26.7 ± 0.7
Average Skin	25.0 ± 0.3

Table 5.3 The measured absorbed dose of pelvis scan for initial setting protocol (1660 mAs).

Position	**Mean absorbed dose (mGy ± SD)**
Rectum	37.0 ± 1.4
Right ovary	34.8 ± 1.2
Left ovary	32.4 ± 0.9
Anterior skin	39.2 ± 1.0
Right lateral skin	30.8 ± 2.5
Left lateral skin	27.1 ± 2.4
Posterior skin	35.6 ± 4.9
Average Skin	33.2 ± 1.7

5.2 Determination of the relationship between absorbed dose and total tube current-time (mAs)

The relationship between total mAs setting and absorbed dose for chest and pelvis scan was determined. For various mAs protocols, the organ and skin dose were shown in Table 5.4-5.5 for chest and pelvis, respectively. Total mAs were reduced from the initial setting protocols in three steps which are 75, 50 and 25 %. The maximum dose at heart for chest scan was reduced to 25.6, 15.7 and 7.90 mGy when using 832, 520 and 260 total mAs, respectively. The rectum dose in pelvis scan was reduced to 29.9, 19.7 and 10.1 mGy when using 1300, 832 and 416 total mAs, respectively.

Figure 5.5-5.8 represent the relationships between total mAs setting and organ absorbed dose for chest and pelvis protocols, respectively. The relation was a linear relationship with R^2 more than 0.9 for all cases. The linear equations for calculating the organ dose were appeared in each line in the figure 5.5-5.8 where Y is absorbed dose in cGy and X is the total mAs setting for the image acquisition. The comparisons for each skin site of anterior, right lateral, left lateral and posterior for chest and pelvis scan were shown in Figure 5.9-5.10. The skin dose for anterior is similar to posterior and the skin dose for right site was more than left site for both protocols. Equations for calculating the average skin dose were shown in the figures where Y is the absorbed dose in cGy and X is the total mAs setting for the image acquisition.

The equations for calculating absorbed dose was $Y=0.003X-0.026$, $Y=0.002X-0.13$, $Y=0.002X-0.233$ and $Y=0.002X-0.0278$ for heart, right breast, left breast and average skin of chest scan, respectively. For pelvis scan, the equations were $Y=0.002X+0.077$, $Y=0.002X+0.078$, $Y=0.002X-0.0278$ and $Y=0.002X+0.106$ for rectum, right ovary, left ovary and average skin for pelvis scan, respectively. The relationship between the total mAs setting and absorbed dose was found to be a linear in which R^2 was more than 0.9 for all cases so the mAs setting was directly affecting to the dose measurement. Therefore, the linear relationships reported in this study can be used as a quick reference for estimating the organ and skin dose when different mAs is used.

Table 5.4 The mean absorbed dose of organ and skin by using various mAs protocol for chest scan.

Position	Mean absorbed dose (mGy ± SD)		
	832 mAs	**520 mAs**	**260 mAs**
Heart	25.6 ± 0.5	15.7 ± 0.6	7.98 ± 0.7
Right breast	22.2 ± 0.9	12.7 ± 0.2	5.84 ±0.4
Left breast	18.2 ± 0.9	11.5 ± 0.1	3.05 ± 0.2
Anterior skin	21.8 ± 0.6	12.9 ± 0.9	4.22 ± 0.7
Right lateral skin	19.3 ± 0.6	11.5 ± 0.6	3.51 ± 0.1
Left lateral skin	16.8 ± 1.1	9.90 ± 0.4	2.01 ± 0.1
Posterior skin	22.9 ± 0.3	12.7 ± 0.5	5.42 ± 0.8
Average Skin	20.2 ± 0.2	11.8 ± 0.2	3.89 ± 0.9

Table 5.5 The mean absorbed dose of organ and skin by using various mAs protocol for pelvis scan.

Position	Mean absorbed dose (mGy ± SD)		
	1300 mAs	**832 mAs**	**416 mAs**
Rectum	29.9 ± 1.5	19.7 ± 0.8	1.01 ± 0.1
Right ovary	28.1 ± 1.9	18.5 ± 0.9	0.95 ± 0.1
Left ovary	28.4 ± 1.1	17.8 ± 0.6	0.93 ± 0.1
Anterior skin	29.3 ± 2.6	21.0 ± 1.6	1.07 ± 0.4
Right lateral skin	26.8 ± 2.0	17.6 ± 1.0	0.89 ± 0.2
Left lateral skin	22.7 ± 2.7	14.5 ± 1.2	0.74 ± 0.4
Posterior skin	32.0 ± 1.4	20.0 ± 1.0	1.00 ± 0.2
Average Skin	27.7 ± 1.7	18.3 ± 1.1	0.92 ± 0.1

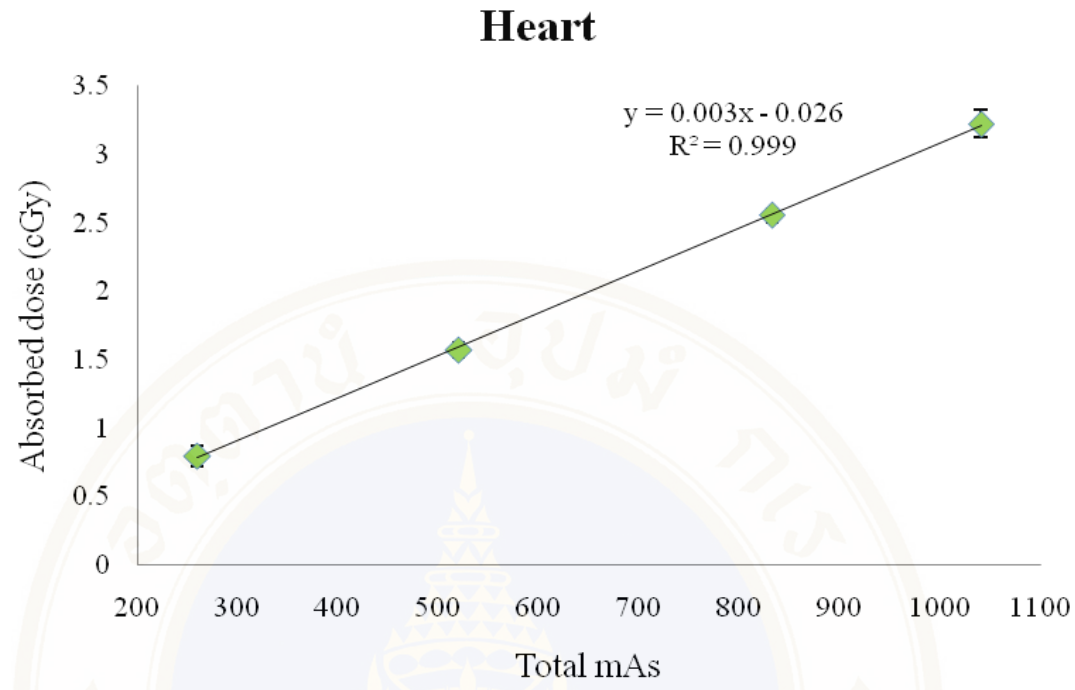

Figure 5.5 The relationship between absorbed dose (cGy) and total mAs setting at heart for chest scan.

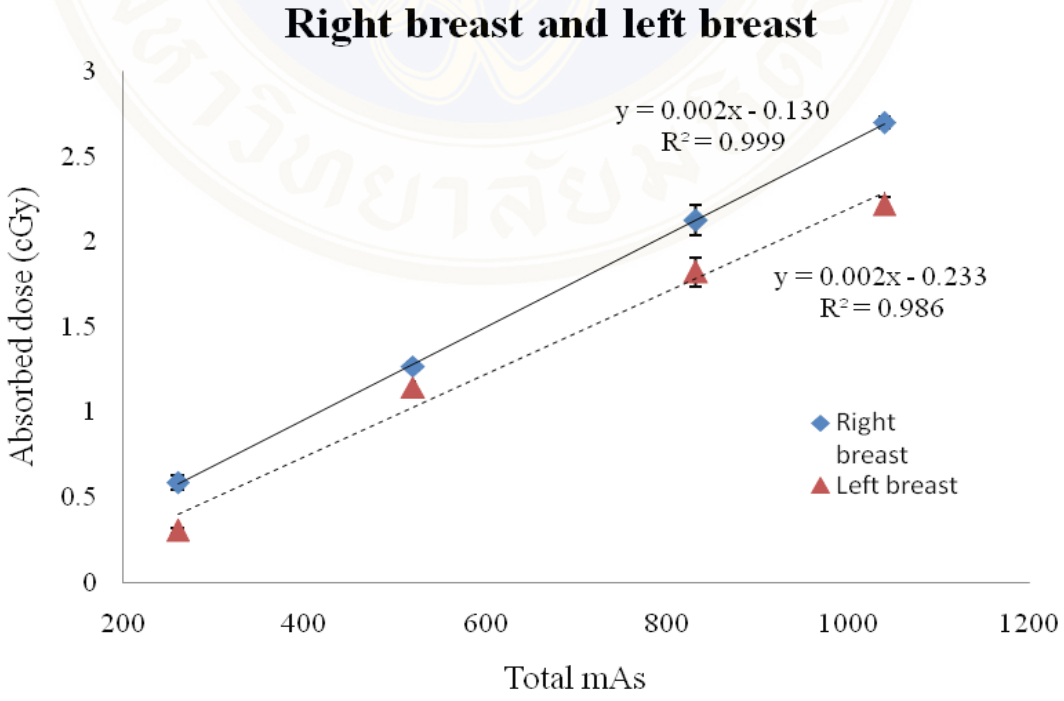

Figure 5.6 The relationship between absorbed dose (cGy) and total mAs setting at right and left breast for chest scan.

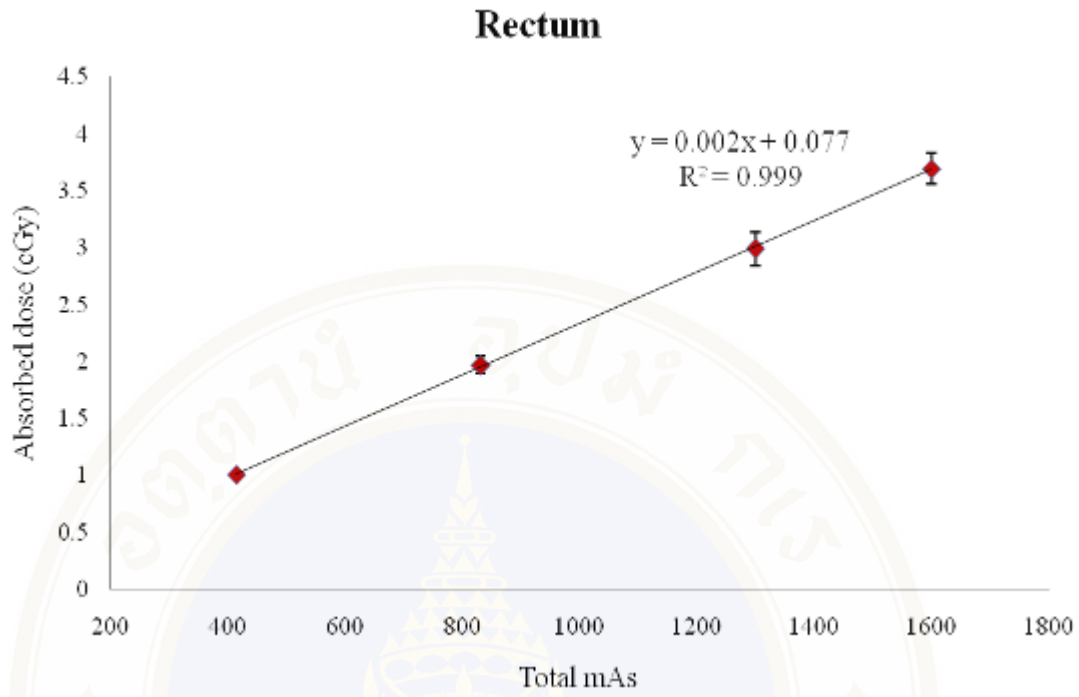

Figure 5.7 The relationship between absorbed dose (cGy) and total mAs setting at rectum for pelvis scan.

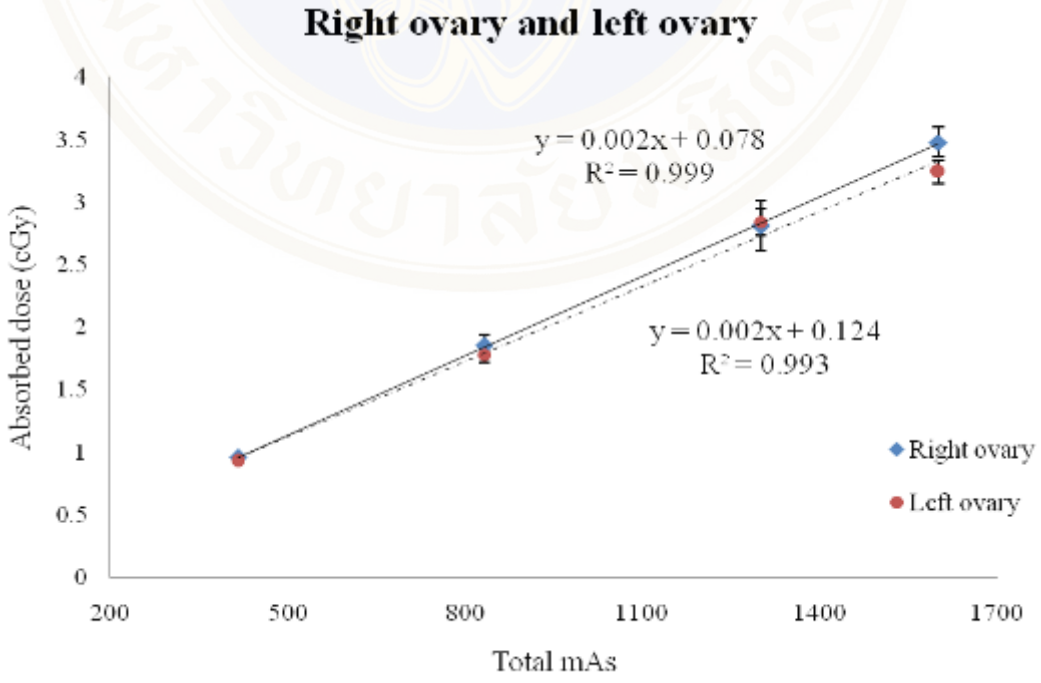

Figure 5.8 The relationship between absorbed dose (cGy) and total mAs setting at right and left ovaries for pelvis scan.

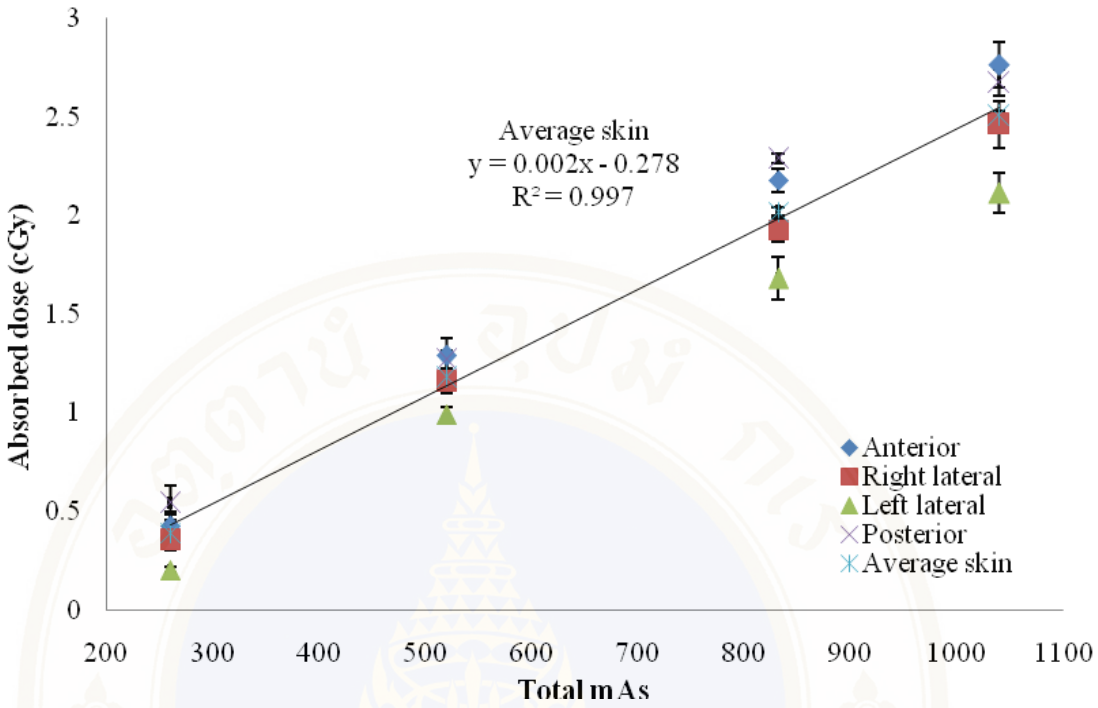

Figure 5.9 The relationship between absorbed dose (cGy) of average skin and total mAs setting for chest scan.

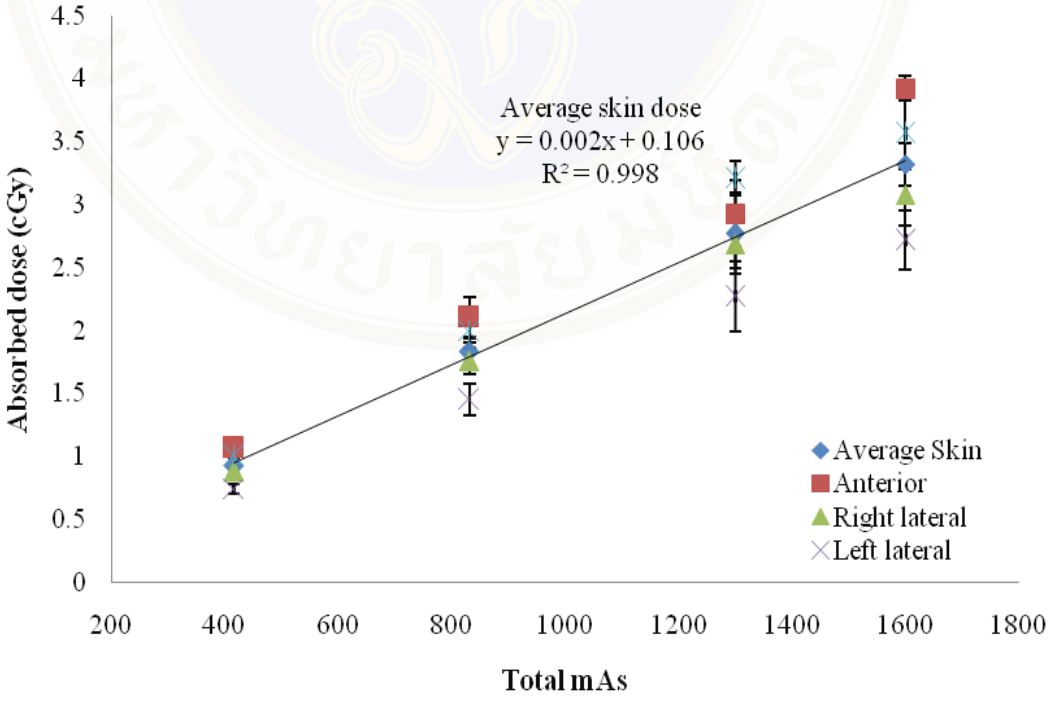

Figure 5.10 The relationship between absorbed dose (cGy) of average skin and total mAs setting for pelvis scan.

The dose measurement in organ and skin in this study can be comparable to the data measured by Amer A. et al. as shown in Table 5.6. However some comparisons of dose measured data were problematic because the imaging acquisition used differently total mAs setting.

Table 5.6 The comparison of measured dose for organ and skin from the literature.

Site	**Position**	**Amer A. et al.**		**This study (cGy) (Initial protocol)**		**This study (cGy) (Various mAs protocol)**	
		mAs	(mGy)	mAs	(mGy)	mAs	(mGy)
Head and neck	Eye lens	38	1.3	36.1	12	-	-
	Anterior skin	38	1.3	36.1	1.2	-	-
	Lateral skin	38	1.2	36.1	1.3	-	-
Chest	Heart	152	7.2	1040	32.2	260	7.9
	Anterior skin	152	10	1040	27.6	260	4.2
	Lateral skin	152	7	1040	22.9	260	2.8
Pelvis	Rectum	-	-	1664	37.0	416	10.1
	Anterior skin	456	34	1664	39.2	416	10.7
	Lateral skin	456	23	1664	29.0	416	8.20

5.3 Image quality test

Figure 5.11-5.28 showed the transverse image of Catphan® 503 for analyzed image quality in low contrast visibility, high contrast resolution and noise. The results of image quality test in low contrast visibility, high contrast resolution and noise were shown in Table 5.7 for 10 and 20 cm collimator sizes, respectively. For all setting parameters of kV-CBCT acquisition, two collimators size, 10 and 20 cm in length were used. The results of low contrast visibility for collimator size 10 cm and 20 cm were between 1-1.84 and 1.11-4.4%, respectively. The highest low contrast visibility was 4.4% for head and neck protocol by using collimator size 20 cm. The highest spatial resolution of 6 lp/cm was obtained with the collimator size 10 cm for head and neck protocol. For chest and pelvis, high contrast resolution was found as 2-3 lp/cm and 4-5 lp/cm for collimator size 10 and 20 cm, respectively. The high contrast resolution was found to be equal between initial and various mAs protocol but the acquisition by using collimator size 10 cm was shown better than that of collimator size 20 cm. Noise was ranged 2.75-7.28 for chest and pelvis scan. For head and neck, noise was 21.59 and 24.88 for the collimator size 10 and 20 cm, respectively.

Table 5.7 The results of image quality test for the collimator size 10 cm and 20 cm.

Technique setting	**Total mAs**	**Low contrast visibility (%)**		**High contrast resolution (lp/cm)**		**Noise (SD)**	
		10*	**20***	**10***	**20***	**10***	**20***
Head and neck	36.1	1.7	4.4	6	5	21.59	24.88
Chest	1040	1.38	1.11	5	3	4.19	4.74
	832	1.17	1.19	4	3	4.34	4.98
	520	1.15	1.21	4	2	4.18	7.28
	260	1.58	1.68	4	3	5.55	6.86
Pelvis	1660	1.00	1.35	4	3	3.41	3.96
	1300	1.03	1.49	4	3	4.4	2.75
	832	1.17	1.19	4	3	4.34	4.98
	416	1.84	1.61	5	3	4.5	6.27

* Collimator size (cm)

a) 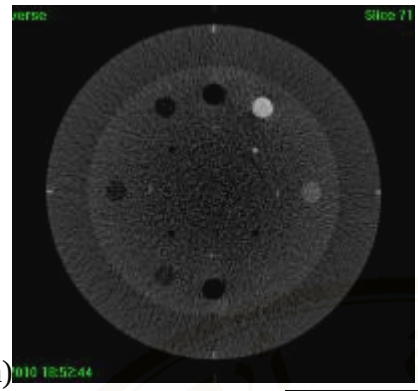 b) 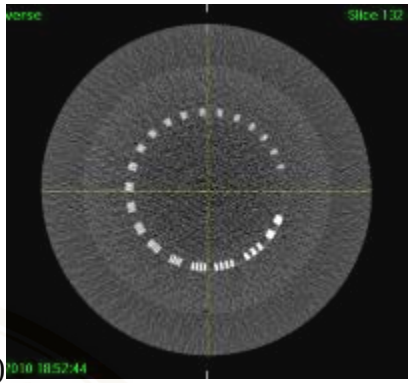

c) 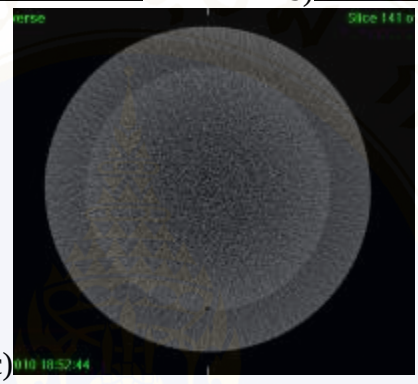

Figure 5.11 The image quality test of head and neck 36.1 mAs by using collimator 10 cm a) low contrast visibility, b) high contrast resolution and c) noise.

a) 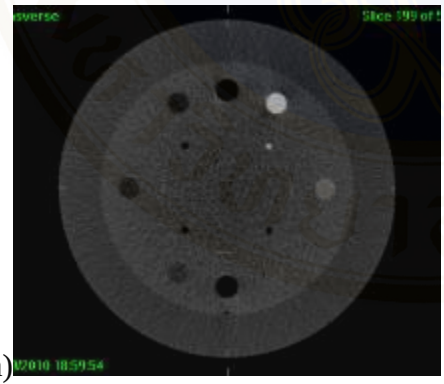 b) 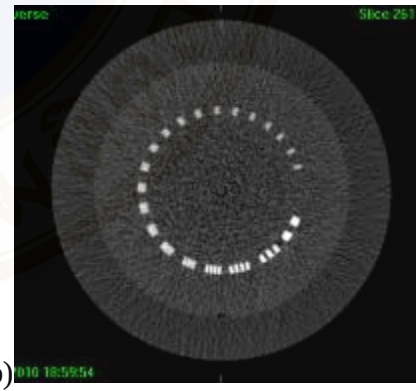

c) 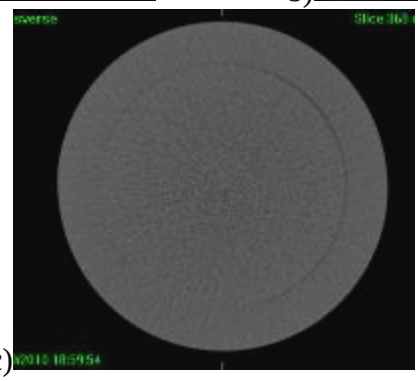

Figure 5.12 The image quality test of head and neck 36.1 mAs by using collimator 20 cm a) low contrast visibility, b) high contrast resolution and c) noise.

a) 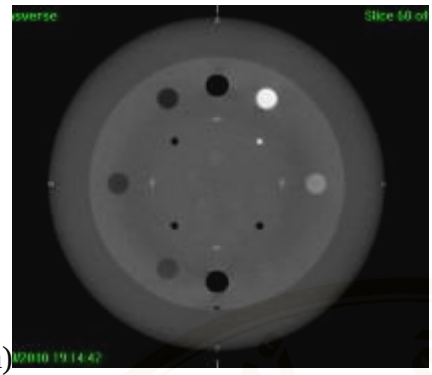 b) 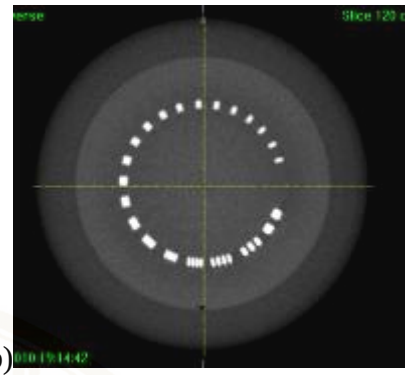

c) 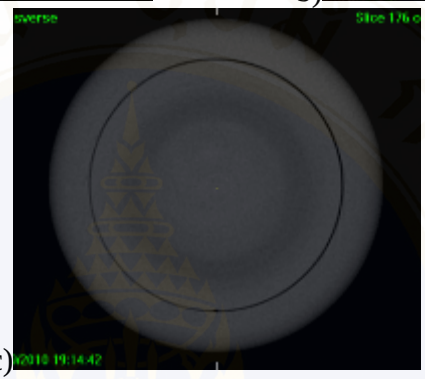

Figure 5.13 The image quality test of chest 1040 mAs by using collimator 10 cm a) low contrast visibility, b) high contrast resolution and c) noise.

a) 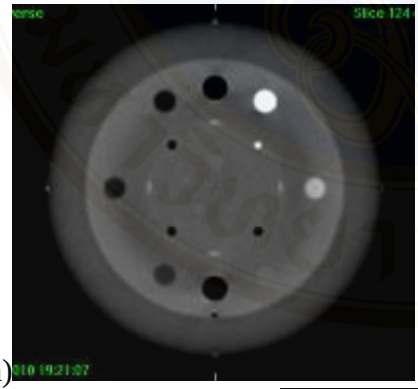 b) 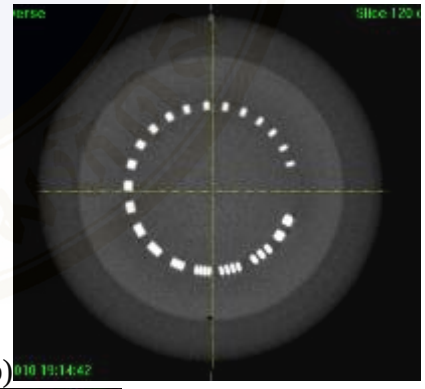

c) 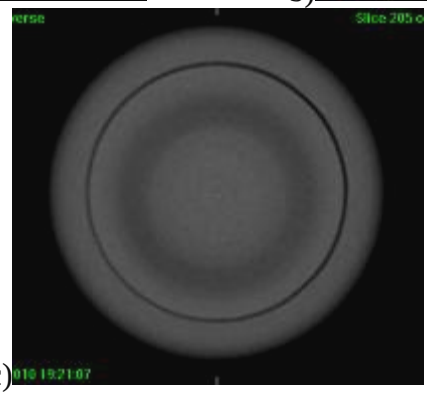

Figure 5.14 The image quality test of chest 1040 mAs by using collimator 20 cm a) low contrast visibility, b) high contrast resolution and c) noise.

a) 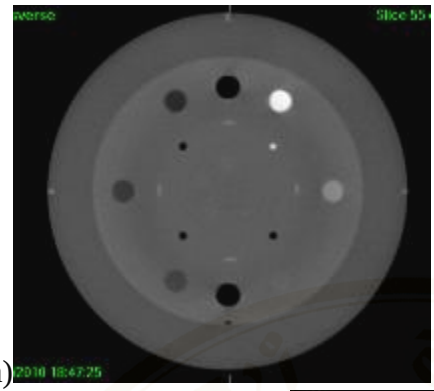 b) 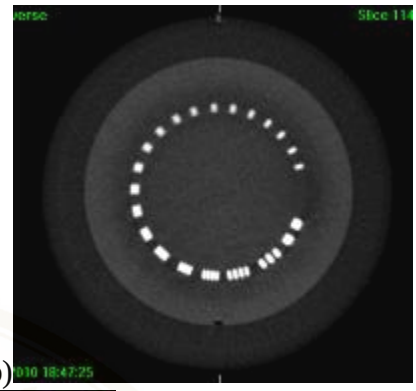

c) 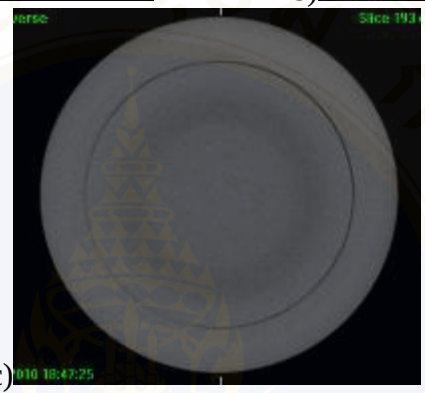

Figure 5.15 The image quality test of chest 832 mAs by using collimator 10 cm a) low contrast visibility, b) high contrast resolution and c) noise.

a) 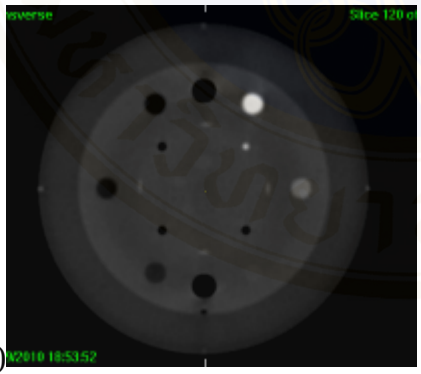 b) 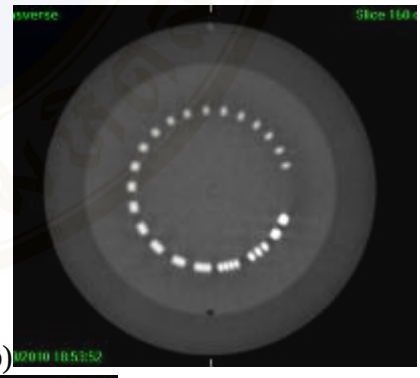

c) 

Figure 5.16 The image quality test of chest 832 mAs by using collimator 20 cm a) low contrast visibility, b) high contrast resolution and c) noise.

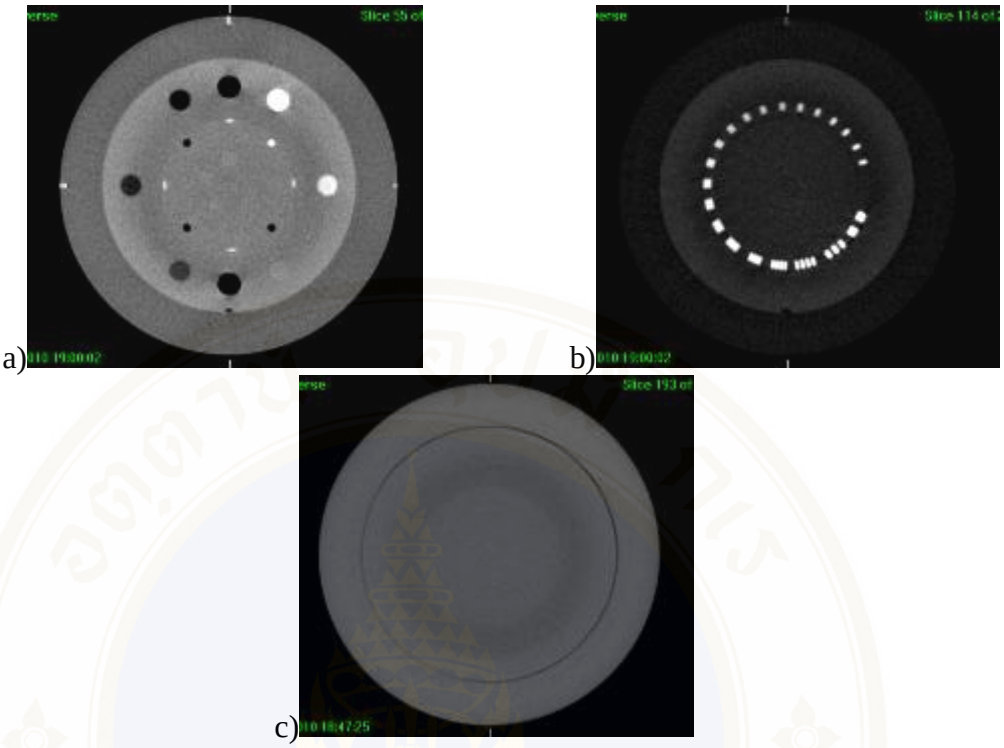

Figure 5.17 The image quality test of chest 520 mAs by using collimator 10 cm a) low contrast visibility, b) high contrast resolution and c) noise.

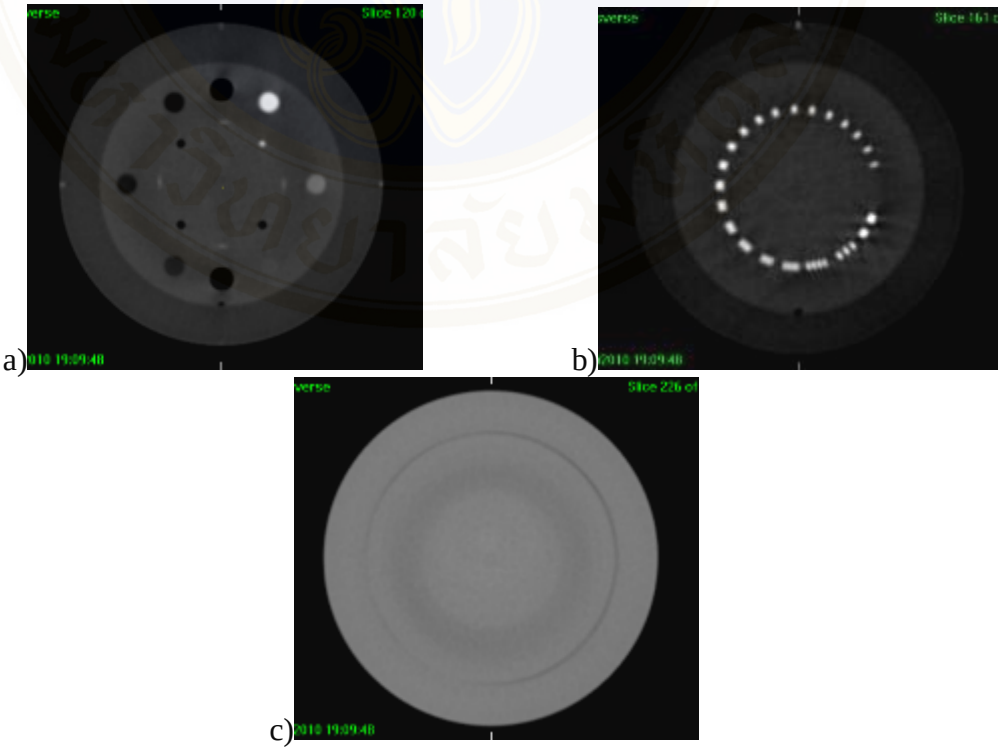

Figure 5.18 The image quality test of chest 520 mAs by using collimator 20 cm a) low contrast visibility, b) high contrast resolution and c) noise.

a) 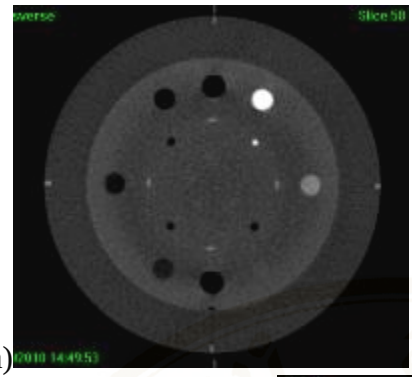 b) 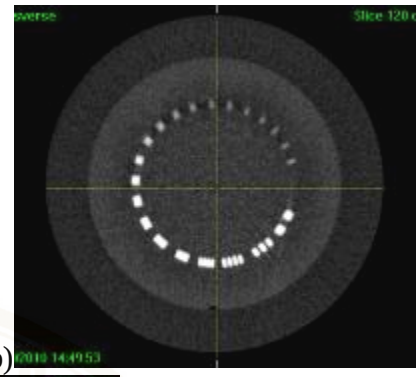

c) 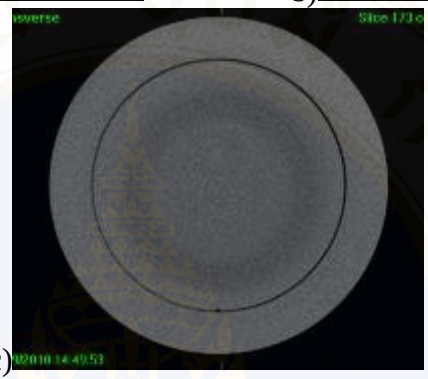

Figure 5.19 The image quality test of chest 260 mAs by using collimator 10 cm a) low contrast visibility, b) high contrast resolution and c) noise.

a) 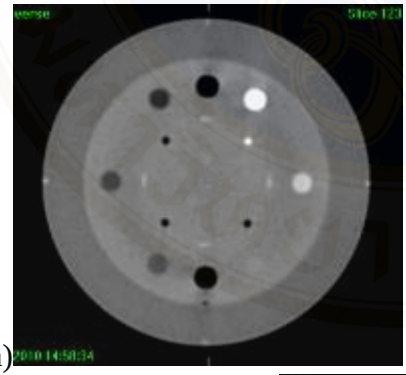 b) 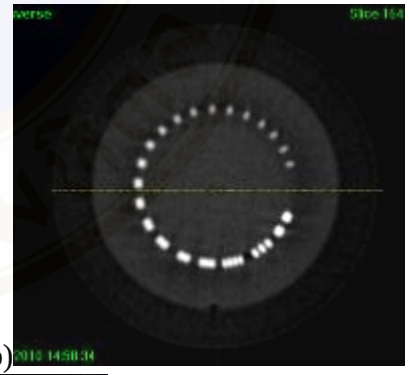

c) 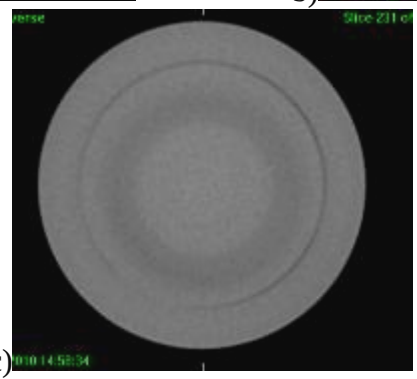

Figure 5.20 The image quality test of chest 260 mAs by using collimator 20 cm a) low contrast visibility, b) high contrast resolution and c) noise.

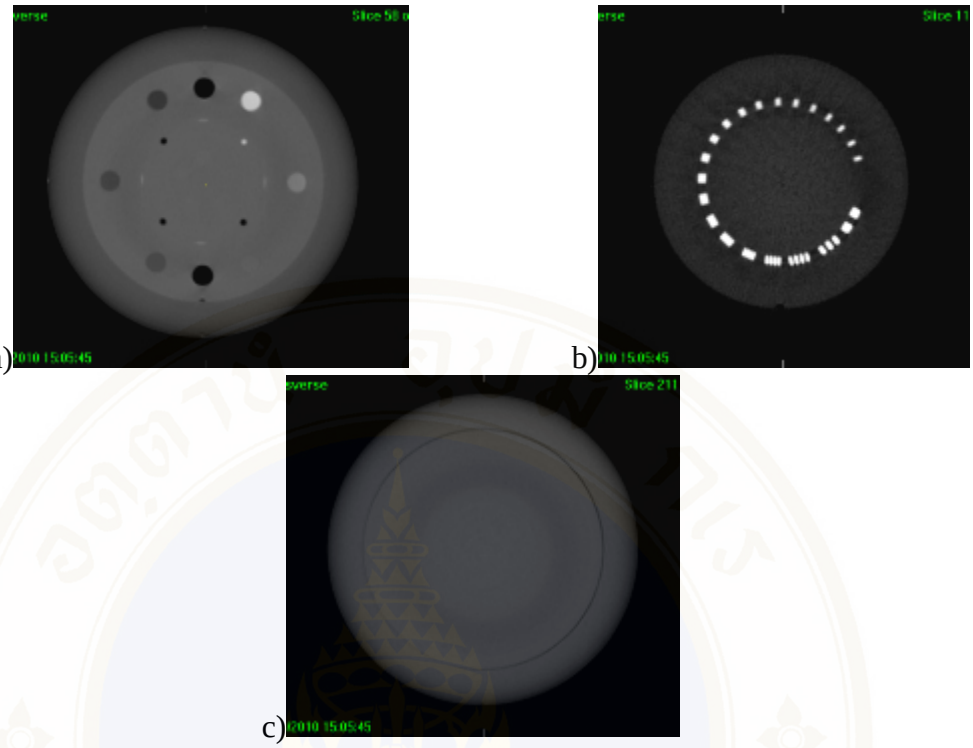

Figure 5.21 The image quality test of pelvis 1660 mAs by using collimator 10 cm a) low contrast visibility, b) high contrast resolution and c) noise.

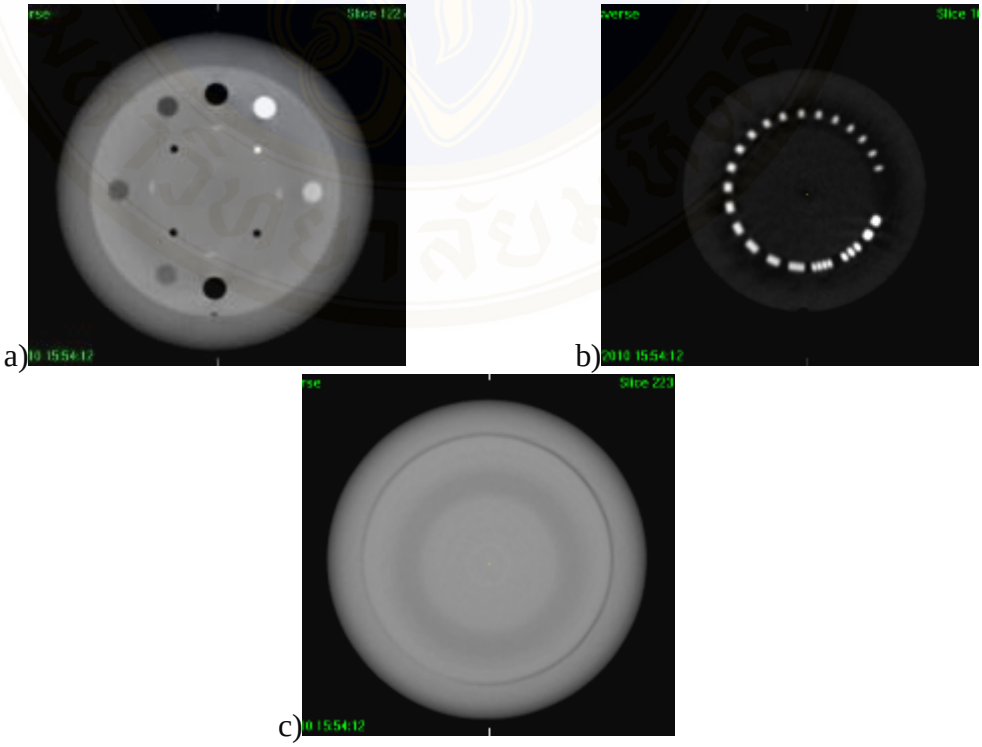

Figure 5.22 The image quality test of pelvis 1660 mAs by using collimator 20 cm a) low contrast visibility, b) high contrast resolution and c) noise.

a) 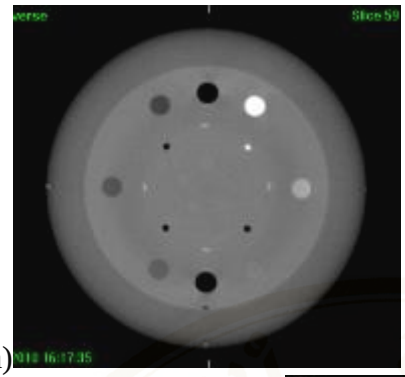 b) 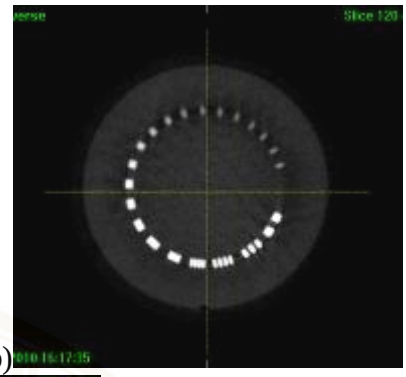

c) 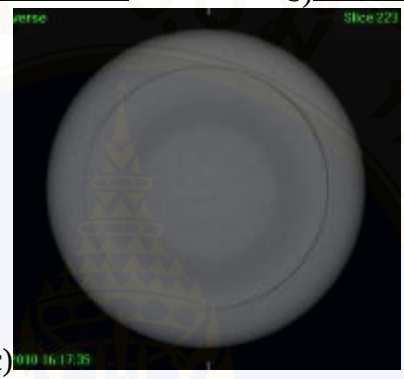

Figure 5.23 The image quality test of pelvis 1300 mAs by using collimator 10 cm a) low contrast visibility, b) high contrast resolution and c) noise.

a) 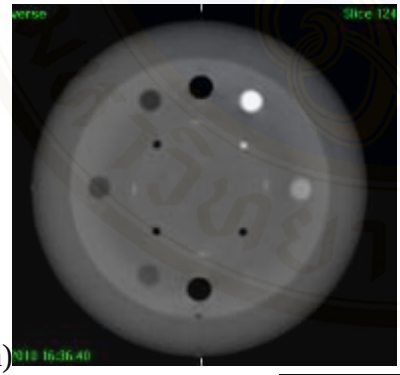 b) 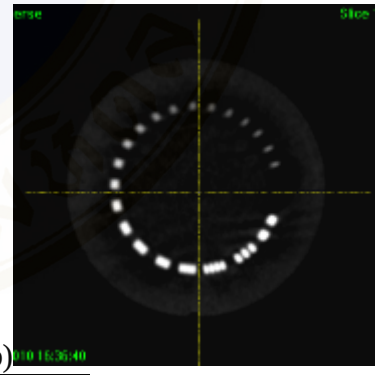

c) 

Figure 5.24 The image quality test of pelvis 1300 mAs by using collimator 20 cm a) low contrast visibility, b) high contrast resolution and c) noise.

a) 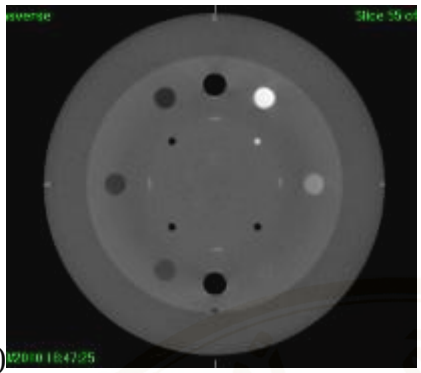 b) 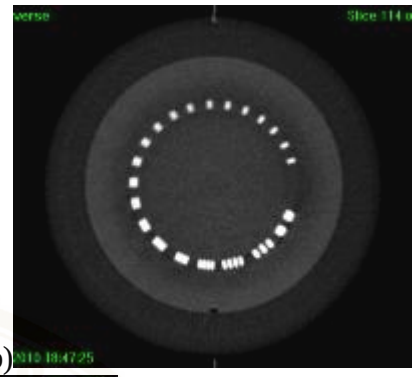

c) 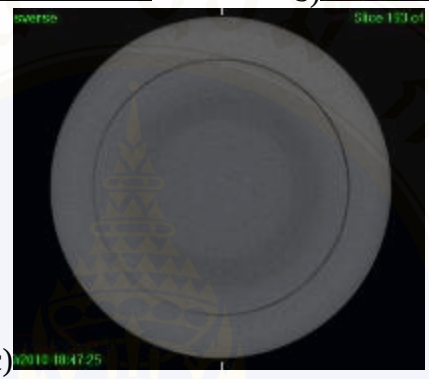

Figure 5.25 The image quality test of pelvis 832 mAs by using collimator 10 cm a) low contrast visibility, b) high contrast resolution and c) noise.

a) 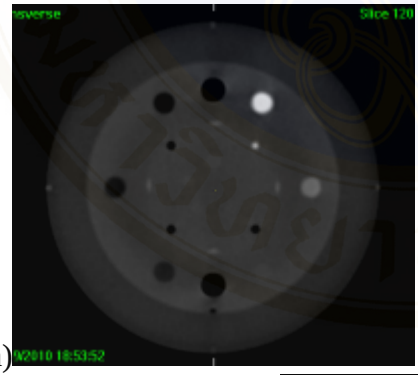 b) 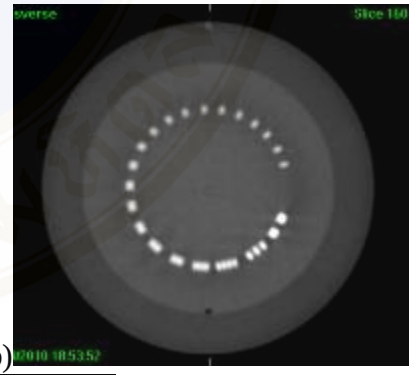

c) 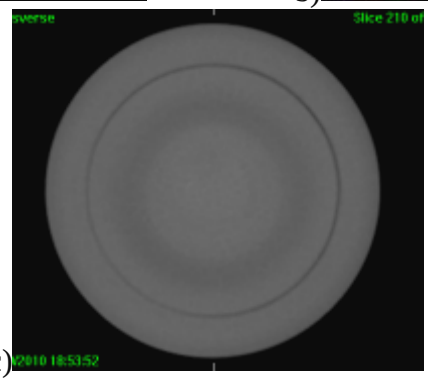

Figure 5.26 The image quality test of pelvis 832 mAs by using collimator 20 cm a) low contrast visibility, b) high contrast resolution and c) noise.

a) 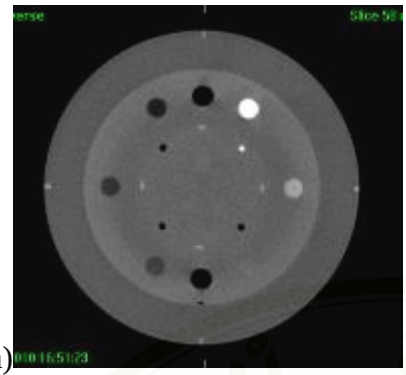 b) 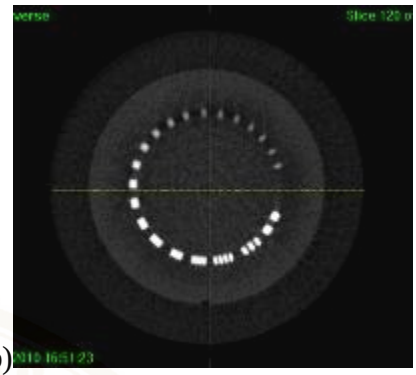

c) 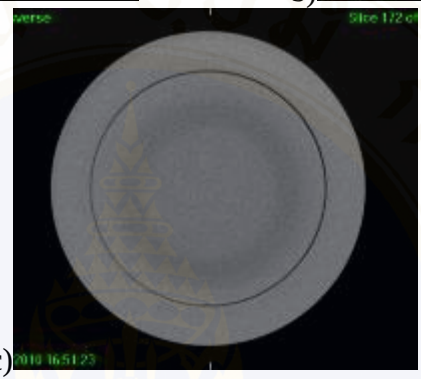

Figure 5.27 The image quality test of pelvis 416 mAs by using collimator 10 cm a) low contrast visibility, b) high contrast resolution and c) noise.

a) 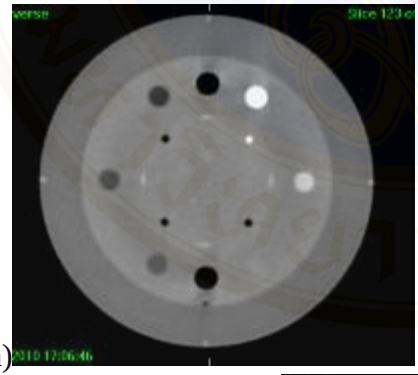 b) 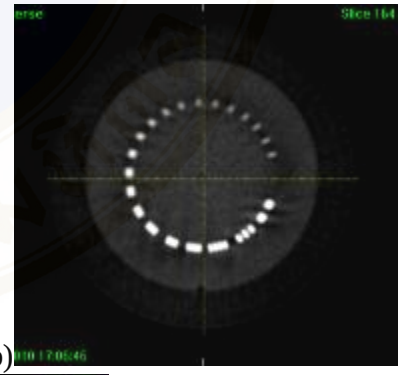

c) 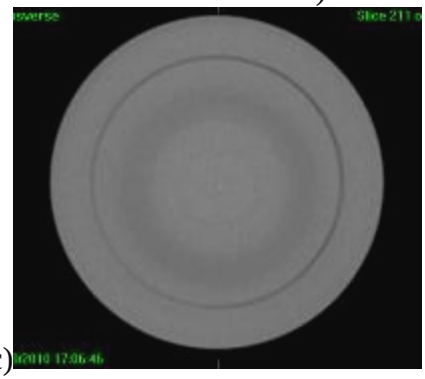

Figure 5.28 The image quality test of pelvis 416 mAs by using collimator 20 cm a) low contrast visibility, b) high contrast resolution and c) noise.

The comparison of low contrast visibility, high contrast resolution and noise for collimator size 10 and 20 cm were shown in Figure 5.29-5.31. The low contrast visibility for collimator size 20 cm of 36.1 mAs was shown as the highest value of 4.4% and quite different from collimator size 10 cm. Therefore the small collimator size can improve low contrast visibility of head and neck protocol. For chest and pelvis protocol, low contrast visibility was found to be equal between collimator size 10 and 20 cm. The high contrast resolution for collimator size10 cm was higher than collimator size 20 cm for all total mAs settings. Noise of image from collimator size 20 cm was higher than collimator size 10 cm especially lower mAs setting but 1300 mAs setting showed differently. Therefore image quality depends on the collimator size of the image acquisition. The small collimator size for image acquisition could be improved image quality to obtain higher contrast resolution and lower noise.

For head and neck, the acquisition of low mAs setting showed much noise because the image was acquired by using 180 degree but it is sufficient to show the bony detail to register with the planning image for positioning verification. Therefore the mAs setting of head and neck in initial setting scan could be appropriate for image registration. However the requirement for the visualization of tumors or soft tissue structures in the chest and pelvis is high mAs technique. Therefore the dose reduction for chest and pelvis imaging significantly affected on image quality. The image quality test of two different collimator sizes showed that the small collimator can improve the image quality. Therefore image quality depend on collimator size, if higher image quality is obtained, smaller size of collimator is needed. Acquisition kV-CBCT images with small field size not only to improve the image quality but also to reduce the additional dose at the region outside the field. The image from various mAs techniques could be sufficient to use for image registration.

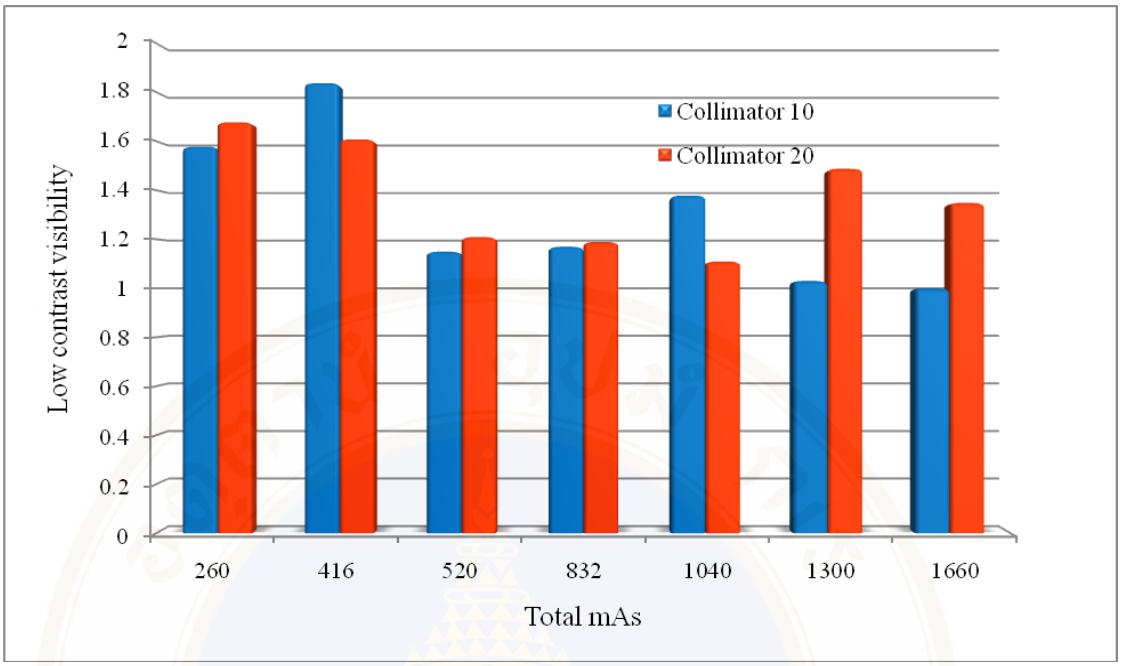

Figure 5.29 The comparison of low contrast visibility for collimator size 10 and 20 cm.

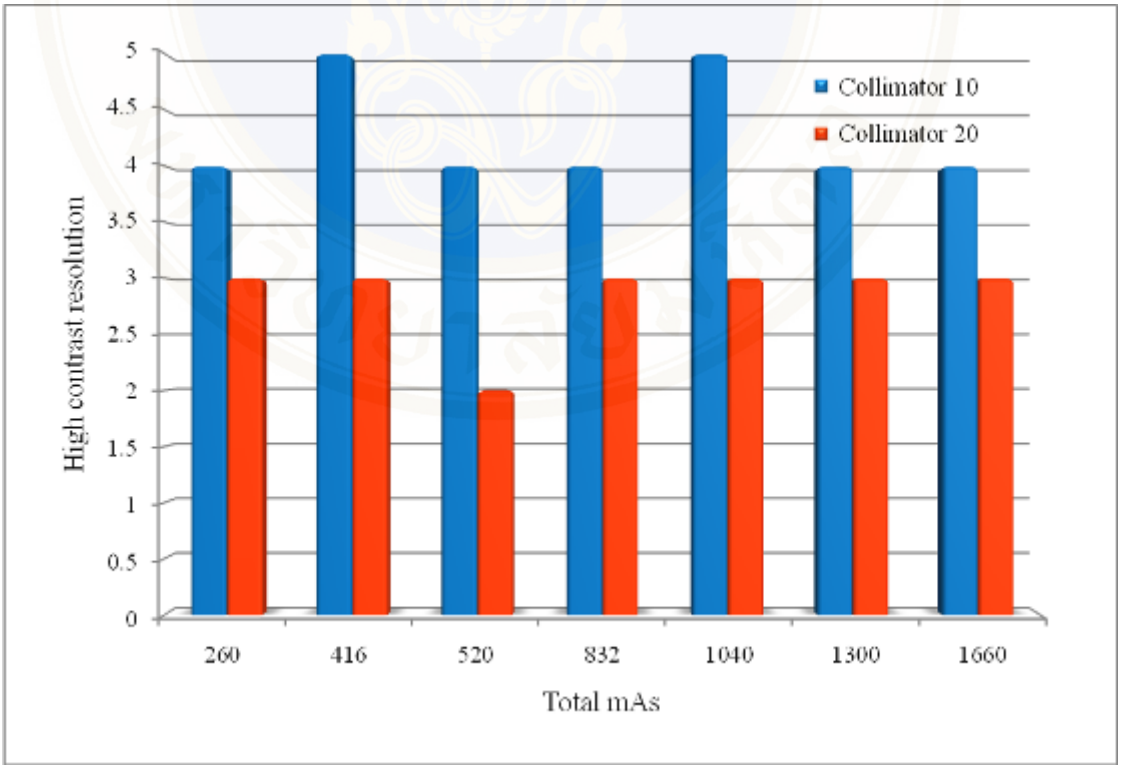

Figure 5.30 The comparison of high contrast resolution for collimator size 10 and 20 cm.

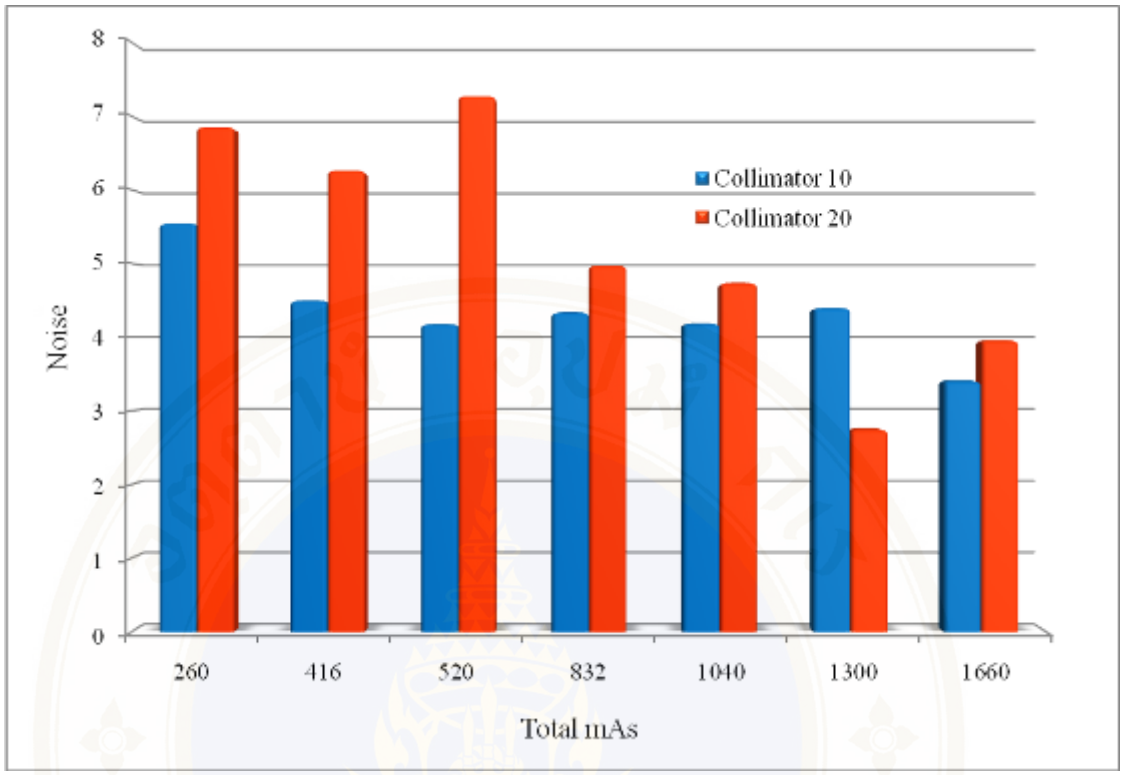

Figure 5.31 The comparison of noise for collimator size 10 and 20 cm.

CHAPTER VI
CONCLUSIONS

The absorbed dose measurement of kV-CBCT for the initial protocol at three different sites; head and neck, chest and pelvis by using TLDs was found that the maximum dose at anterior skin for pelvis was 39.2 mGy. For a typical whole treatment course of 35 fractions, the skin dose could be 1.37 Gy. However, this skin dose value is still within the deterministic level of 2 Gy for transient skin erythema (14).

The maximum organ dose for head and neck, chest and pelvis was found at thyroids, heart and rectum which were 1.3, 32.2 and 37.0 mGy, respectively. The total dose of eye lens and ovaries in 35 fractions was 0.09 and 1.18 Gy. However, the total dose in 35 fractions of eye lens and ovaries was less than 5 and 6 Gy for the threshold dose of detectable opacities and sterility in ICRP 103 (15), respectively.

Moreover, the study found that various mAs settings were linearly to the dose measurement with $R^2 > 0.9$ for all cases thus if the total mAs setting is reduced, the dose will be reduced at the same rate. The study found that, for chest and pelvis scan, when total mAs was reduced from the initial setting protocol to 75, 50 and 25 percent , the maximum absorbed dose for chest was 32.2 mGy at heart and was reduced to 25.6, 15.7 and 7.98 mGy, respectively. The maximum absorbed dose for pelvis scan at the initial setting protocol was 37.0 mGy for rectum and was reduced to 29.9, 19.7 and 10.1 mGy, respectively. It was determined that the dose decreased quite linearly as the total mAs setting was decreased. Therefore linear relationships of absorbed dose and total mAs in this study can be used as a quick reference for estimating the absorbed dose for different mAs settings.

The data of dose measurement and image quality can be used for considering the mAs setting techniques for optimization protocol. Therefore the recommendation of the total mAs for the optimizing protocol of chest and pelvis scan should be 832 and 1300 mAs, respectively while maintaining the image quality. The smaller size of collimator could improve the quality of image by making contrast resolution higher and noise lower.

REFERENCES

1. Xing L, Thorndyke B, Schreibmann E, Yang Y, Li T, Kim G, Luxton G, Koong A. Overview of image-guided radiation therapy. Med Dosim 2006; 31: 91-112.
2. Gayou O, Miften M. Commissioning and clinical implementation of a mega-voltage cone beam CT system for treatment localization. Med Phys 2007;34:3183-92
3. Kan MWK, Leung LHT, Wong W and Lam N. Radiation dose from cone beam computerd tomography for Image-Guided Radiation Therapy. Int. J. Radiat Oncol Biol Phys 2008; 70: 272-279.
4. Murphy MJ, Balter J, Balter S, Das IJ, Jiang B, et al. The management of imaging dose during image-guided radiotherapy: Report of the AAPM Task Group 75. Med Phys 2007;34: 4041–4063.
5. Amer A, Marchant T, Sykes J, Czajka J, and Moore C. Imaging doses from the Elekta Synergy X-ray cone beam CT system. Br J Radiol 2007; 80: 476-482.
6. Kan MWK, Leung LHT, Wong W and Lam N. Radiation dose from cone beam computed tomography for Image-Guided Radiation Therapy. Int. J. Radiat Oncol Biol *Phys* 2008; 70: 272-279.
7. Song WY, Kamath S, Ozawa S, et al. A dose comparison study between XVI® and OBI® CBCT systems. *Med Phys* 2008; 35: 480-486.
8. Kim S, Yoshizumi T, Toncheva G, et al. Comparison of radiation doses between cone beam CT and multi detector CT: TLD measurements. *Radiat. Prot. Dosim.* 2008; 132: 339-345.
9. Lehmann J, Perks J, Semon S, Harse R, Purdy JA. Commissioning experience with cone-beam computed tomography for image-guided radiation therapy. Journal of applied clinical medical physics 2007; 8: 21-36.
10. Harshaw Dicron. Automatic TLD Reader User's Manual, Saint-Gobain/Norton Industrial Ceramics CO., Ohio, 1993.
11. Lawrence HL, The RANDO phantom and its medical application. ARL Inc., Illinois, 1973.

12. The Phantom Laoratory, Incorporated. Catphan® 503 Manual, Newyork, 2010.
13. Elekta Limited. Clinical User Manual for XVI R4.0, England, 2006.
14. Valentin J. Radiation and your patient: a guide for medical practitioners: ICRP Supporting Guidance 2. Annals ICRP 2001;31:1.
15. ICRP 103. Recommendations of the International Commission of Radiological Protection, Annals ICRP 2007.

APPENDIX

APPENDIX A
THE CORRECTION FACTOR FOR SENSITIVITY OF EACH TLD

The correction factor for sensitivity of each TLD was show in Table A1. The TLDs that used for the absorbed dose measurement have correction factor for sensitivity values varied from 0.9206 - 1.0996.

Table A1. Correction factor (CF) for sensitivity of each TLD

TLD NO.	CF	TLD NO.	CF	TLD NO.	CF	TLD NO.	CF
1	1.0996	22	1.0279	43	0.9759	64	0.9492
2	1.0995	23	1.0270	44	0.9755	65	0.9481
3	1.0818	24	1.0221	45	0.9752	66	0.9479
4	1.0797	25	1.0192	46	0.9730	67	0.9442
5	1.0778	26	1.0177	47	0.9723	68	0.9439
6	1.0749	27	1.0172	48	0.9719	69	0.9419
7	1.0732	28	1.0169	49	0.9675	70	0.9390
8	1.0727	29	1.0158	50	0.9668	71	0.9382
9	1.0709	30	1.0122	51	0.9659	72	0.9364
10	1.0692	31	1.0102	52	0.9658	73	0.9349
11	1.0674	32	1.0045	53	0.9635	74	0.9326
12	1.0651	33	0.9899	54	0.9618	75	0.9313
13	1.0645	34	0.9897	55	0.9613	76	0.9290
14	1.0604	35	0.9895	56	0.9606	77	0.9258
15	1.0563	36	0.9889	57	0.9592	78	0.9227
16	1.0478	37	0.9873	58	0.9591	79	0.9206
17	1.0465	38	0.9868	59	0.9577		
18	1.0351	39	0.9853	60	0.9527		
19	1.0346	40	0.9845	61	0.9522		
20	1.0319	41	0.9836	62	0.9505		
21	1.0295	42	0.9798	63	0.9504		

BIOGRAPHY

NAME	Miss Nunthawadee Teocharoen
DATE OF BIRTH	11 November 1980
PLACE OF BIRTH	Bangkok, Thailand
INSTITUTION ATTENDED	Mahidol University, 2001; Bachelor of Science (Radiological Technology) Mahidol University, 2011; Master of Science (Medical Physics)
HOME ADDRESS	92/9 M1 Bangkrang, Muang, Nonthaburi, Thailand 11000 Tel. 0-2447-3733